Ribosome stalling caused by the Argonaute-miRNA-SGS3 complex regulates production of secondary siRNA biogenesis in plants

Hiro-oki Iwakawa[1,2,*], Andy Y.W. Lam[1,3], Akira Mine[2,4,5], Tomoya Fujita[6,7], Kaori Kiyokawa[1], Manabu Yoshikawa[8], Atsushi Takeda[4,5], Shintaro Iwasaki[3,6], Yukihide Tomari[1,3].

[1] Laboratory of RNA Function, Institute for Quantitative Biosciences, The University of Tokyo, Bunkyo-ku, Tokyo 113-0032, Japan.

[2]JST, PRESTO, Saitama 332-0012, Japan.

[3]Department of Computational Biology and Medical Sciences, Graduate School of Frontier Sciences, The University of Tokyo, Bunkyo-ku, Tokyo 113-0032, Japan.

[4]Ritsumeikan Global Innovation Research Organization, Ritsumeikan University, Kusatsu, Shiga 525-8577, Japan.

[5]Department of Biotechnology, Graduate School of Life Sciences, Ritsumeikan University, Shiga 525-8577, Japan.

[6]RNA Systems Biochemistry Laboratory, RIKEN Cluster for Pioneering Research, Wako, Saitama, 351-0198 Japan.

[7]School of Life Science and Technology, Tokyo Institute of Technology, Yokohama, Kanagawa, 226-8503 Japan.

[8]Division of Plant and Microbial Sciences, Institute of Agrobiological Sciences, National Agriculture and Food Research Organization, 2-1-2 Kannondai Tsukuba, Ibaraki 305-

8602, Japan.

*Correspondence: iwakawa@iqb.u-tokyo.ac.jp (H.-o.I)

Abstract

The path of ribosomes on mRNAs can be impeded by various obstacles. One such example is halting of ribosome movement by microRNAs, though the exact mechanism and physiological role remain unclear. Here, we find that ribosome stalling caused by the Argonaute-miRNA-SGS3 complex regulates production of secondary siRNA biogenesis in plants. We show that the double-stranded RNA-binding protein, SGS3, directly interacts with the 3′ end of the microRNA-Argonaute complex, resulting in ribosome stalling. Strikingly, microRNA-mediated ribosome stalling enhances production of secondary small interfering RNAs (siRNAs) from target mRNAs. Our results uncover a previously uncharacterized role for paused ribosomes in regulation of small RNA function that may have broad biological implications across the plant kingdom.

Main

Ribosome movement can be interrupted by various factors including rare codons, special RNA structures and specific amino acid sequences called ribosome arrest peptides[1,2]. Although the physiological roles of such impediments are unclear, growing evidence indicates that ribosome stalling has diverse functions, including ER stress response, monitoring protein secretion, feedback regulation of methionine biosynthesis, quality control of mRNAs, and folding of nascent peptide chains[2–4].

Recent findings suggested that microRNAs (miRNAs) can cause ribosome stalling as well as target RNA degradation or cleavage[5–10]. To pause ribosomes, miRNAs need to form RNA-induced silencing complexes (RISCs) with Argonaute (AGO) protein, and extensively base-pair within the coding sequence (CDS) of the target mRNA[5,6,9]. However, these requirements are not sufficient for ribosome stalling in plants; although many plant miRNAs have their cleavable targets with perfect or near perfect complementary binding sites in CDS, only a few miRNA binding sites can induce ribosome stalling *in vivo*[9]. Thus, unknown elements other than RISC binding should be required for miRNA-mediated ribosome pausing.

The biological function of the miRNA-mediated ribosome stalling also remains unclear. One plausible role of the miRNA-mediated ribosome stalling is inhibition of functional protein synthesis[5–7]. However, given that the target cleavage activity of plant RISC is functionally sufficient to silence target gene expression, ribosome stalling may have a role other than translation repression.

Here, we show that a dsRNA binding protein, SGS3, is a key determinant of miRNA-mediated ribosome stalling. SGS3 forms a complex on dsRNA protruding from the miR390-AGO7-target complex. These mechanisms also operate in the context of a distinct 22-nucleotide miRNA-AGO1-RISC complex. Importantly, we find that SGS3 and miRNA-mediated ribosome stalling enhances amplification of RNA silencing, revealing a new role of ribosome pausing beyond inhibition of protein synthesis.

Results

The dsRNA-binding protein SGS3 is a specific enhancer for microRNA-mediated ribosome stalling

We sought to find the miRNA-mediated ribosome stalling positions in a genome-wide scale. To do this, we first performed ribosome profiling, an approach that is based on sequencing of ribosome-protected footprints after RNase treatment[11], in *Arabidopsis* seedlings. Our data represented a 3-nucleotide periodicity along the ORF, a hallmark of translation elongation (Extended Data Fig. 1a). We combined this high-resolution ribosome profiling and the miRNA target prediction[12] to identify the ribosome-stalling position upstream of the predicted miRNA binding sites (Supplementary Table 1). Along with earlier studies[8–10], our ribosome profiling has shown that specific miRNAs, including miR390 and miR173, can induce ribosome stalling 12–13 nucleotide upstream of their binding sites in *Arabidopsis thaliana* (Fig. 1a, b, c, Extended Data Fig. 1b, c and d). These particular miRNAs are known to trigger the production of phased secondary small interfering RNAs (siRNAs), called trans-acting siRNAs (tasiRNAs), from precursors

called TAS RNAs[13]. tasiRNA production requires various factors including AGO7 and AGO1, which form specific RISCs with miR390 and miR173, respectively[13–15]. One important factor for tasiRNA biogenesis is SUPPRESSOR OF GENE SILENCING 3 (SGS3)[16–20]. Given that SGS3 forms cytoplasmic foci named "siRNA bodies" with AGO7 (ref. 20) and interacts with miR173-AGO1 RISC (ref. 21), we reasoned that SGS3 influences miRNA-mediated ribosome stalling. To test this idea, we examined the impact of an SGS3 mutation on miRNA-mediated ribosome stalling by comparing ribosome profiling in wild-type and *sgs3-11 Arabidopsis* seedlings[19]. We observed dramatic decreases in ribosome stalling in *sgs3-11* mutants (Fig. 1b and c and Extended Data Fig. 1b, c, d and 2). This reduction cannot be explained by a change in mRNA or miRNA abundance in the mutant (Fig. 1b and c and Extended Data Fig. 1, 2 and 3). Thus, we concluded that SGS3 is required for ribosome stalling by miR390 and miR173. Given that *sgs3-11* mutation did not cause an overall decrease in ribosome occupancy (Extended Data Fig. 2), SGS3 is not a general ribosome stalling factor, but rather a specific stalling enhancer for miRNA-mediated ribosome stalling.

SGS3 and RISC cooperatively stall ribosomes *in vitro*

Although our ribosome profiling data demonstrate the involvement of SGS3 and miRNAs in ribosome stalling, how these factors coordinately pause ribosomes was unclear. To reveal the mechanisms of miRNA- and SGS3-dependent ribosome stalling, we adopted a tobacco BY-2 cell-free system, which can recapitulate miRNA-mediated RNA silencing *in vitro* (Fig. 2a)[6,22]. We used TAS3a as a representative target RNA. TAS3a contains a

short (51 codon) ORF and two miR390-binding sites: one is adjacent to the stop codon and immediately downstream of the ribosome stalling site, and the other is located well downstream of those elements (Fig. 2b)[23]. Ribosome stalling within the short ORF was monitored by detecting peptidyl-tRNAs, a hallmark of ribosome stalling, by western blotting to a FLAG-tag inserted in the F-TAS3 ORF (Fig. 2a and c). Western blotting followed a neutral pH gel electrophoresis that prevents hydrolysis of the ester linkage between the tRNA and amino acid[24], thus enabling us to detect peptidyl-tRNAs within stalled ribosomes through an ~18 kDa upshift —the size of the tRNA moiety (Fig. 2c). Translation of the reporter (F-TAS3) in the presence of AGO7-RISC led to a clear band-shift (Fig. 2d and e). Disappearance of this signal after RNase treatment confirmed that the upshifted band corresponds to peptidyl-tRNA (Fig. 2d).

The two miR390-binding sites in TAS3a are functionally distinct; the 5′ possesses central mismatches that preclude RISC-mediated target cleavage but allow stable binding, whereas the 3′ miR390 binding site is centrally matched with the miR390 and thus cleaves the TAS3a RNA (Fig. 2b)[23]. The adjacent 5′ binding site is essential for ribosome stalling. Mutations in the “seed region”, which is critical for miRNA recognition, of the 3′ miR390 binding site (Fig. 2b, F-TAS3_3M) did not impair ribosome stalling, whereas also mutating the 5′ binding site (Fig. 2b, F-TAS3_5M_3M) reduced stalling (Fig. 2d and e). Thus, ribosome stalling requires base-pairing between miR390 in AGO7-RISC and the 5′ miR390-binding site in TAS3a. As the 3′ site mutation increased peptidyl-tRNA accumulation, presumably by stabilizing the mRNA since it is no longer cleaved (Fig. 2d), we decided to use F-TAS3_3M for further experiments.

We next sought to investigate the impact of SGS3 on ribosome stalling. Because endogenous SGS3 (NtSGS3) is abundant in BY-2 cells[21], we immuno-depleted NtSGS3 from the lysate (Fig. 2f) and found decreased ribosome stalling (Fig. 2g and h). Supplementing with recombinant AtSGS3 markedly rescued ribosome stalling efficiency (Fig. 2f, g and h), indicating that SGS3 is a critical and limiting factor for miRNA-mediated ribosome stalling. Taken altogether, our *in vitro* system faithfully recapitulated ribosome stalling triggered by AGO7-RISC and SGS3.

SGS3 binding to the 3′ end of initiator microRNAs is required for ribosome pausing

The functional roles of AGO7-RISC and SGS3 prompted us to hypothesize that these two factors form a complex that promotes ribosome stalling. SGS3 is an RNA-binding protein that preferentially binds RNA duplexes with a 5′ overhang[25]. In theory, such a substrate is formed between the 3′ end of miR390 within AGO7 and the 5′ end of the miR390-binding site. We therefore hypothesized that SGS3 directly interacts with the end of the dsRNA protruding from AGO7. To test this scenario, we first examined the interaction between SGS3 and AGO7-RISC. The FLAG-tagged AGO7 mRNA was translated in the BY-2 cell lysate, then the miR390 duplex was added to program RISC. After further incubation with TAS3 mRNAs, the reaction mixture was used for co-immunoprecipitation with anti-FLAG antibody (Fig. 3a). This assay revealed that endogenous NtSGS3 binds AGO7-RISC only in the presence of both miR390 and TAS3 variants with a wild-type 5′ site (Extended Data Fig. 4a). Remarkably, introducing mismatches at the 5′ end of the miR390-binding site (Fig. 3b, TAS3_5endM_3M) or using

a miR390 variant that is one-nucleotide shorter (20 nt) (Fig. 3b), which is not predicted to protrude from AGO7, disrupted the interaction between NtSGS3 and AGO7-RISC (Fig. 3b, c, d, Extended Data Fig. 4b). These results strongly support a model where SGS3 forms a complex with AGO7-RISC via dsRNA with a 5′ overhang formed at the 3′ end of miR390.

To test whether SGS3 directly interacts with the 3′ end of miR390 on the *TAS3* RNA, we performed a site-specific UV crosslinking assay, in which molecules neighboring the 3′ end of miR390 can be captured. We first substituted the 3′ end cytidine of miR390 with a photo-reactive 4-thiouridine (Extended Data Fig. 4c, miR390_4SU), and restored base-pairing using a TAS3a variant with a G-to-A substitution at the 5′ miR390 binding site (Extended Data Fig. 4c, TAS3_G21A_3M). This variant successfully rescued the interaction between miR390_21_4SU-loaded AGO7 and NtSGS3 (Extended Data Fig. 4c and d). In this context of the reporter, proteins crosslinked to 5′ radiolabeled miR390_21_4SU were separated on an SDS-PAGE gel (Fig. 3e). In the absence of the target RNA, a specific band appeared at around 120 kDa (Fig. 3f, red arrowhead). Immunoprecipitation using the anti-FLAG antibody revealed that the band corresponds to F-AGO7 (Fig. 3g, red arrowheads). Strikingly, addition of the target RNA changed the crosslinked protein from AGO7 to a ~90 kDa protein, which, verified as NtSGS3 using immunoprecipitation (Fig. 3f and h). These results indicate that target binding alters protein interactions at the 3′ end of miR390, switching them from AGO7 to SGS3, likely via conformational changes in AGO7-RISC.

To test if the physical interaction between SGS3 and AGO7-RISC is critical for ribosome pausing, we performed *in vitro* ribosome stalling experiments under conditions where SGS3 fails to bind AGO7-RISC using reporter variant F-TAS3_5endM_3M or the short 20-nt version of miR390. In both cases, stalling efficiencies were significantly decreased (Fig. 3i, j, k and l). Taken together, we find a direct interaction between SGS3 and the 3′ end of 21-nt miR390 bound to AGO7-RISC is necessary for ribosome stalling on TAS3 mRNA.

It is worth noting that the required length of miRNA for SGS3 binding and ribosome pausing may differ between partner AGO proteins. In contrast to AGO7, AGO1—bound by most miRNAs—requires a 22-nt long miR173 for both SGS3 interaction and ribosome stalling (Fig. 4a, b, c and d) [21]. As miRNAs are typically 21-nt long, plants may have evolved a AGO1 structure that fully encapsulates the 21-nt miRNAs, thus limiting promiscuous SGS3 binding and ribosome stalling. Importantly, we find that ribosome pausing occurs even if TAS1 is cleaved by AGO1-RISC loaded with 22-nt miR173 (Fig. 4d and e). This is not limited to the TAS1 and miR173-AGO1 pair. AGO7-miR390-SGS3 complex also stalls ribosomes on the cleavable binding site which has perfect complementarity to miR390 (Extended Data Fig. 5a, b and c). Because AGO-miRNA-SGS3 complex holds and stabilizes both 5′ and 3′ RNA fragments after target cleavage (Fig. 4e)[21], we reasoned that SGS3 and RISC can stay on the cleaved targets long enough to stall ribosomes.

Ribosome stalling enhances the production of secondary siRNAs

The striking requirement of a TAS precursor structure for ribosome stalling (Fig. 1a, b and c, Extended Data Fig. 1b, c, d) led us to hypothesize that ribosome pausing by the SGS3-miRNA complex promotes tasiRNA production. So far, several studies have focused on the relationship between translation and tasiRNA biogenesis[8–10,26,27]. However, it is still controversial if positioning of the miRNA-binding site in the CDS or near the stop codon is important for tasiRNA production[8,26,27]. For example, previous quantitative RT-PCR (qRT-PCR) experiments showed no significant changes in tasiRNA production between the wild-type TAS3 and a mutant TAS3 that possesses an early stop codon located far upstream of the 5′ miR390 binding site[8], suggesting that ribosome stalling has no impact on the tasiRNA biogenesis. To carefully assess the impact of ribosome stalling on tasiRNA biogenesis, we first attempted to construct TAS3 variants with no ribosome stalling that retain binding to AGO7 and SGS3. Such variants were obtained by inserting 4 or more nucleotides between the stop codon and 5′ miR390 binding site in TAS3 (Fig. 5a, b and Extended Data Fig. 6). As ribosomes stall one-codon upstream of the stop codon in TAS3, we reasoned that these insertions promote normal translation termination without interfering in the binding between AGO7-RISC and SGS3.

To test the hypothesis that ribosome pausing promotes the production of tasiRNAs, we compared tasiRNA accumulation in different TAS3 variants in *Nicotiana benthamiana* leaves. We opted to use Northern blotting for accurate detection of the secondary siRNAs, because this method can distinguish the canonical secondary siRNAs from the non-specific RNA fragments derived from the TAS3 reporters by size. Co-expression of miR390 and AGO7 efficiently produced 21-nt tasiRNAs, compared with

the 5′ miR390 binding site mutant (TAS3_5M) (Fig. 5c, d and e). Thus, our transient assay successfully recapitulated canonical TAS3 tasiRNA biogenesis. Importantly, placing the 5′ miR390 binding site 6-nucleotide away (Fig. 5c, TAS3+6) significantly reduced tasiRNA production to ~60% (Fig. 5d and e), suggesting that clearance of stalled ribosomes impairs efficient tasiRNA production. In contrast, tasiRNA production from a TAS3 variant with a 3-nucleotide insertion (Fig. 5c, TAS+3), which still stalls ribosomes, was comparable to that from wild-type TAS3 (Fig. 5d and e). To confirm if ribosome stalling enhances the tasiRNA biogenesis, we introduced artificial tandem stop codons at the ~120 nt upstream of the miR390 target site (early_stop), which forces ribosomes to terminate without stalling (Fig. 5c). In contrast to the previous report [8], our quantitative Northern blotting revealed that the tandem early stop codons significantly reduced tasiRNA production to ~60%, similarly to TAS3+6 (Fig. 5d and e). These data were not explained by changes in precursor *TAS3* abundance (Fig. 5f and g). Altogether, we conclude that ribosome stalling regulates secondary siRNA production in a manner different from stabilization of mRNAs.

Discussion

Here, we find that the dsRNA-binding protein SGS3 forms ribosome stalling complexes on the protruding end of the dsRNA formed between the TAS RNAs and miR390-AGO7 or 22-nt miR173-AGO1-RISC (Fig. 6). In general, the ribosome displaces RNA binding proteins bound to mRNAs during elongation[28], suggesting that SGS3 imposes an extreme barrier for trailing ribosomes. A recent study suggested that unconventional base-pairing

234 between human miRNAs and target sites cause transient ribosome stalling[5]. Although the
235 precise stalling mechanism remains unclear in animals, there may be an RNA-binding
236 protein(s) that protects the 3′ end of miRNA from the helicase activity of ribosomes.
237 Strikingly, we demonstrate that ribosome stalling is a regulator for tasiRNA
238 biogenesis (Fig.5d, e and 6). This is supported from an evolutionary standpoint; most
239 plant species have the 5′ miR390 binding site just downstream the stop codon or in the
240 CDS of TAS3 (Supplementary Table 2). The molecular details of how ribosome stalling
241 enhances tasiRNA production warrant future studies. Given that arrest peptide-mediated
242 ribosome-pausing induces changes in mRNA localization in animal cells[29], we suggest
243 that miRNA-mediated ribosome pausing may promote to deliver the tasiRNA precursors
244 to a secondary siRNA "factory", such as the siRNA body[20].
245 We observed SGS3- and RISC-dependent ribosome stalling in five TAS loci in
246 *Arabidopsis* (Fig. 1). However, they must be just a tip of the iceberg of miRNA-mediated
247 ribosome pausing. There are many DNA regions named PHAS loci that produce phased
248 secondary siRNAs (phasiRNAs) by the same mechanism as TAS loci[13]. Although our
249 ribosome profiling failed to detect obvious ribosome stalling 11–14 nt upstream of
250 miRNA binding sites in known PHAS loci (Fig. 1 and Supplementary Table 1), more
251 sensitive methods like single-molecule imaging[30] may reveal ribosome stalling on the
252 miRNA-bound targets. In addition to miRNAs, siRNAs may also induce ribosome
253 stalling. A recent study demonstrates that 22-nt siRNAs, which have the potential to
254 recruit SGS3, accumulate upon environmental stress, trigger the RNA silencing
255 amplification, and mediate translational repression[31]. Such 22-nt siRNAs are also induced

256 by viral infection[16,32–35]. Therefore, SGS3- and miRNA/siRNA-mediated ribosome
257 stalling is likely to have an impact on a wider range of cellular processes such as stress
258 adaptation and antiviral immunity in plants.

259

260

Main references

1. Schuller, A. P. & Green, R. Roadblocks and resolutions in eukaryotic translation. *Nat Rev Mol Cell Biol* **19**, 526-541 (2018).
2. Ito, K. & Chiba, S. Arrest peptides: cis-acting modulators of translation. *Annu Rev Biochem* **82**, 171-202 (2013).
3. Stein, K. C., Kriel, A. & Frydman, J. Nascent Polypeptide Domain Topology and Elongation Rate Direct the Cotranslational Hierarchy of Hsp70 and TRiC/CCT. *Mol Cell* **75**, 1117-1130.e5 (2019).
4. Inada, T. The Ribosome as a Platform for mRNA and Nascent Polypeptide Quality Control. *Trends Biochem Sci* **42**, 5-15 (2017).
5. Zhang, K. et al. A novel class of microRNA-recognition elements that function only within open reading frames. *Nat Struct Mol Biol* (2018).
6. Iwakawa, H. O. & Tomari, Y. Molecular Insights into microRNA-Mediated Translational Repression in Plants. *Mol Cell* **52**, 591-601 (2013).
7. Iwakawa, H. O. & Tomari, Y. The Functions of MicroRNAs: mRNA Decay and Translational Repression. *Trends Cell Biol* **25**, 651-665 (2015).
8. Bazin, J. et al. Global analysis of ribosome-associated noncoding RNAs unveils new modes of translational regulation. *Proc Natl Acad Sci U S A* **114**, E10018-E10027 (2017).
9. Hou, C. Y. et al. Global Analysis of Truncated RNA Ends Reveals New Insights into Ribosome Stalling in Plants. *Plant Cell* **28**, 2398-2416 (2016).
10. Li, S. et al. Biogenesis of phased siRNAs on membrane-bound polysomes in Arabidopsis. *Elife* **5**, e22750 (2016).
11. Ingolia, N. T., Ghaemmaghami, S., Newman, J. R. & Weissman, J. S. Genome-wide analysis in vivo of translation with nucleotide resolution using ribosome profiling. *Science* **324**, 218-223 (2009).
12. Dai, X., Zhuang, Z. & Zhao, P. X. psRNATarget: a plant small RNA target analysis server (2017 release). *Nucleic Acids Res* **46**, W49-W54 (2018).
13. Fei, Q., Xia, R. & Meyers, B. C. Phased, secondary, small interfering RNAs in posttranscriptional regulatory networks. *Plant Cell* **25**, 2400-2415 (2013).
14. Montgomery, T. A. et al. Specificity of ARGONAUTE7-miR390 interaction and

dual functionality in TAS3 trans-acting siRNA formation. *Cell* **133**, 128-141 (2008).

15. Endo, Y., Iwakawa, H. O. & Tomari, Y. Arabidopsis ARGONAUTE7 selects miR390 through multiple checkpoints during RISC assembly. *EMBO Rep* **14**, 652-658 (2013).
16. Mourrain, P. et al. Arabidopsis SGS2 and SGS3 genes are required for posttranscriptional gene silencing and natural virus resistance. *Cell* **101**, 533-542 (2000).
17. Allen, E., Xie, Z., Gustafson, A. M. & Carrington, J. C. microRNA-directed phasing during trans-acting siRNA biogenesis in plants. *Cell* **121**, 207-221 (2005).
18. Vazquez, F. et al. Endogenous trans-acting siRNAs regulate the accumulation of Arabidopsis mRNAs. *Mol Cell* **16**, 69-79 (2004).
19. Peragine, A., Yoshikawa, M., Wu, G., Albrecht, H. L. & Poethig, R. S. SGS3 and SGS2/SDE1/RDR6 are required for juvenile development and the production of trans-acting siRNAs in Arabidopsis. *Genes Dev* **18**, 2368-2379 (2004).
20. Jouannet, V. et al. Cytoplasmic Arabidopsis AGO7 accumulates in membrane-associated siRNA bodies and is required for ta-siRNA biogenesis. *EMBO J* **31**, 1704-1713 (2012).
21. Yoshikawa, M. et al. 3' fragment of miR173-programmed RISC-cleaved RNA is protected from degradation in a complex with RISC and SGS3. *Proc Natl Acad Sci U S A* **110**, 4117-4122 (2013).
22. Iki, T. et al. In vitro assembly of plant RNA-induced silencing complexes facilitated by molecular chaperone HSP90. *Mol Cell* **39**, 282-291 (2010).
23. Axtell, M. J., Jan, C., Rajagopalan, R. & Bartel, D. P. A two-hit trigger for siRNA biogenesis in plants. *Cell* **127**, 565-577 (2006).
24. Nakatogawa, H. & Ito, K. Secretion monitor, SecM, undergoes self-translation arrest in the cytosol. *Mol Cell* **7**, 185-192 (2001).
25. Fukunaga, R. & Doudna, J. A. dsRNA with 5' overhangs contributes to endogenous and antiviral RNA silencing pathways in plants. *EMBO J* **28**, 545-555 (2009).
26. Zhang, C., Ng, D. W., Lu, J. & Chen, Z. J. Roles of target site location and sequence complementarity in trans-acting siRNA formation in Arabidopsis. *Plant J* **69**, 217-226 (2012).

27. Yoshikawa, M. et al. A Short Open Reading Frame Encompassing the MicroRNA173 Target Site Plays a Role in trans-Acting Small Interfering RNA Biogenesis. *Plant Physiol* **171**, 359-368 (2016).
28. Halstead, J. M. et al. TRICK: A Single-Molecule Method for Imaging the First Round of Translation in Living Cells and Animals. *Methods Enzymol* **572**, 123-157 (2016).
29. Yanagitani, K., Kimata, Y., Kadokura, H. & Kohno, K. Translational pausing ensures membrane targeting and cytoplasmic splicing of XBP1u mRNA. *Science* **331**, 586-589 (2011).
30. Ruijtenberg, S. et al. mRNA structural dynamics shape Argonaute-target interactions. *Nat Struct Mol Biol* (2020).
31. Wu, H. et al. Plant 22-nt siRNAs mediate translational repression and stress adaptation. *Nature* **581**, 89-93 (2020).
32. Akbergenov, R. et al. Molecular characterization of geminivirus-derived small RNAs in different plant species. *Nucleic Acids Res* **34**, 462-471 (2006).
33. Deleris, A. et al. Hierarchical action and inhibition of plant Dicer-like proteins in antiviral defense. *Science* **313**, 68-71 (2006).
34. Garcia-Ruiz, H. et al. Arabidopsis RNA-dependent RNA polymerases and dicer-like proteins in antiviral defense and small interfering RNA biogenesis during Turnip Mosaic Virus infection. *Plant Cell* **22**, 481-496 (2010).
35. Diaz-Pendon, J. A., Li, F., Li, W. X. & Ding, S. W. Suppression of antiviral silencing by cucumber mosaic virus 2b protein in Arabidopsis is associated with drastically reduced accumulation of three classes of viral small interfering RNAs. *Plant Cell* **19**, 2053-2063 (2007).

Methods

General methods.

Preparation of tobacco BY-2 lysate, substrate mixture (containing ATP, ATP-regeneration system, and amino acid mixture), 1×lysis buffer [30 mM HEPES-KOH (pH 7.4), 100 mM potassium acetate, 2 mM magnesium acetate], and microRNA duplexes (Supplementary Table 3) have been previously described in detail[1]. mRNAs were transcribed *in vitro* from NotI- (for plasmids with the prefix "pBYL-") or XhoI- (for plasmids with the prefix "pUC57-") digested plasmids or PCR products using the AmpliScribe T7 High Yield Transcription Kit (Lucigen), followed by capping with ScriptCap m^7G Capping System (Cell Script). Poly(A)-tails were added to transcripts from pUC57-plasmids or PCR products using the T7 promoter by A-Plus Poly(A) Polymerase Tailing Kit (Cell Script). Anti-AtSGS3 (diluted at 1:3000) and anti-AtAGO7 antibodies (diluted at 1:3000) were raised in rabbits using synthetic peptides (NH_2-MSSRAGPMSKEKNVQGGC-COOH) and (NH_2-IPSSKSRTPLLHKPYHHC-COOH) as antigens respectively, and affinity-purified (Medical & Biological Laboratories).

Plants and growth conditions.

Arabidopsis thaliana wild-type (Col-0) and the *sgs3-11* mutant[2] were used in this study. Seeds were incubated in 70% EtOH at room temperature for 2 min, sterilized with liquid sodium hypochlorite, washed 5 times in sterile water, sown on filter paper (Whatman No.2), laid on Murashige and Skoog (MS)-agar plates (1×MS salt, 1% sucrose, 1% agar,

pH 5.7) and incubated at 4°C for 3 days. After vernalization, the plates were incubated at 22°C for 3 days under continuous LED light (LC-LED450W, TAITEC).

Ribosome profiling.

Briefly, 0.2 g of frozen seedlings and 400 µl of *Arabidopsis* lysis buffer (100 mM Tris-HCl pH 7.5, 40 mM KCl, 20 mM $MgCl_2$, 1 mM DTT, 100 µg/ml cycloheximide and 1% Triton X-100) were crushed into a powder using the Multi-beads shocker (Yasui Kikai). The 3000 × g supernatant of the lysate was mixed with 25 µl of Turbo DNase (Thermo Fisher Scientific) and incubated on ice for 10 min. RNA concentration was measured with a Qubit RNA BR Assay Kit (Thermo Fisher Scientific). Ribosome footprints ranging between 17 and 34 nt were gel-purified and subsequent library preparation were executed as previously described[3,4]. Two libraries from two biological replicates (WT_rep1, WT_rep2, sgs3_rep1 and sgs3_rep2) were sequenced on a HiSeq4000 (Illumina). 24 to 29 nt footprints were mapped onto the TAIR10 *Arabidopsis thaliana* genome sequence, excluding rRNA/tRNAs. Empirically, A-site position was estimated as 11 for 24 nt, 12 for 25 nt, 13 for 26 nt, 14 for 27 nt, 15 for 28 nt, 16 for 29 nt, based on the homogeneous 5′ end of the reads. The relative ribosome occupancy r at position j in an ORF of gene g of length l is defined as follows:

$$r_{gj} = \frac{f_{gj}}{d_{gj}}$$

where

395 $$d_{gj} = \frac{\left(\sum_{i=1}^{l} f_i\right) - f_j}{l - 1}$$

396 f_{gj} is the footprint at position j in a ORF of gene g. r_{gj} is a ratio of f_{gj} to the average
397 footprint across nucleotide positions on the ORF of the same gene, d_{gj}.

398

399 **microRNA target prediction.**

400 The targets of mature *Arabidopsis* microRNA sequences [miRbase (miRbase20) [5,6]] were
401 predicted using the psRNATarget server[7,8] with the following settings: # of top targets =
402 15, Expectation = 3, Seed region = 2-8 nt.

403

404 **RNA-seq.**

405 Total RNA was extracted from seedlings with Trizol (Thermo Fisher Scientific). Library
406 construction and deep sequencing were performed by AnnoRoad in Beijing. Reads were
407 mapped to the transcripts of *Arabidopsis thaliana* (derived from TAIR10, ver. 10 released
408 on 2010 in psRNATarget server[7,8]) by Bowtie2[9]. Sam files were converted to bam files
409 using SAMtools[10] and then to bed files with BEDTools[11]. BEDtools[11] was used to
410 calculate the depth of coverage for every base across mRNAs shown in Fig 1b, c,
411 Extended Data Fig. 1b, c and d.

412

413 **Plasmid construction.**

414 The following constructs used in this study have been previously described: pBYL2[12],
415 pBYL-AGO1[13], pBYL-AGO7[13], pBYL-3×FLAG-AGO7[13], pBYL-3×FLAG-AGO1[13],

pBYL-3×FLAG-SUMO-AtAGO1[14], pAT006[15], pMDC32[16], pMDC-Tas3a[17], pMDC-HA-AGO7[17], pMDC-miR390[17]. The DNA fragments used for plasmid construction are listed in Supplementary Table 4.

pBYL-3×HA

A DNA fragment containing the T7 promoter, 5′ UTR of *Arabidopsis thaliana* alcohol dehydrogenase 1 and 3×HA tag (T7_ADH_5UTR_*3×HA,* Supplementary Table 4) was cloned into XbaI/AscI-digested pBYL2 vector using the HiFi DNA Assembly Cloning kit (New England Biolabs).

pBYL-3×HA-AGO7

A DNA fragment containing AGO7 ORF was amplified by PCR with pBYL-AGO7[13] using primers oligoE1 and oligoE2, digested by AscI, and cloned into AscI-digested pBYL-3×HA vector by ligation.

pBYL-3×HA-AGO1

A PCR fragment with AGO1 ORF following 3×HA tag was amplified by overlap extension PCR with pBYL-AGO1[13] as template using primers oligo1118 and oligo1094. The fragment was cloned into AscI-digested pBYL2 vector via HiFi DNA Assembly Cloning kit (New England Biolabs).

pUC57-TAS3

The TAS3a sequence (AT3G17185.1) following T7 promoter (T7_TAS3a, Supplementary Table 4) was inserted into EcoRV-digested pUC57 vector via GenScript gene synthesis service.

pUC57-F-TAS3

Three DNA fragments were prepared by PCR: TAS3a_5′ UTR fragment amplified from pUC57-TAS3 using primers oligo1062 and oligo1063, 3×FLAG tag sequence amplified using two oligos, oligo1064 and oligo512 and the TAS3a ORF amplified from pUC57-TAS3 using primers, oligo1065 and oligo1066. The three DNA fragments were cloned into SacII/XhoI-digested pUC57-TAS3a via HiFi DNA Assembly Cloning kit (New England Biolabs).

pUC57-F-TAS3_3M

Seven nucleotide mismatches were introduced into the seed sequence of the 3′ miR390 binding site (Fig. 2c) in pUC57-F-TAS3 by site directed mutagenesis using primers oligo1073 and oligo1074.

pUC57-F-TAS3_5M_3M

Seven nucleotide mismatches were introduced into the seed sequence of the 5′ miR390 binding site (Fig. 2c) in pUC57-F-TAS3_3M by site directed mutagenesis using primers oligo 1099 and oligo1100.

460 *pUC57-F-TAS3_3M(+1), pUC57-F-TAS3_3M(+2), pUC57-F-TAS3_3M(+3), pUC57-F-*
461 *TAS3_3M(+4), pUC57-F-TAS3_3M(+5), pUC57-F-TAS3_3M(+6) and pUC57-F-*
462 *TAS3_3M(+7)*

463 One to six nucleotides, as shown in Fig. 5a, were inserted between the stop codon of the
464 short ORF and 5′ miR390 binding site in pUC57-F-TAS3_3M by site directed PCR using
465 primer pairs of oligo1180-oligo1181, oligo1182-oligo1183, oligo1161-oligo1162,
466 oligo1163-oligo1164, oligo1165-oligo1166, oligo1167-oligo1168 and oligo1169-
467 oligo1170, respectively.

468

469 *pEU-6×His-SBP-SUMO-AtSGS3*

470 Two DNA fragments were prepared by PCR: 6×His-SBP-SUMOstar-tag fragment
471 amplified from pASW-SUMO-AtRDR6 (Opt)[18] using oligo1044 and oligo1039 and SGS
472 ORF fragment amplified from cDNA of *Arabidopsis thaliana* using oligoK1 and oligoK2.
473 The two DNA fragments were inserted into EcoRV/SmaI-digested pEU-E01-MCS vector
474 via HiFi DNA Assembly Cloning kit (New England Biolabs).

475

476 *pBYL-3×FLAG-SUMOstar-tag-AGO7*

477 Two PCR products were prepared by PCR: 3×FLAG-SUMOstar-tag fragment amplified
478 from pBYL-3×FLAG-SUMO-AtAGO1[14] using primers oligo955 and oligo1039 and
479 AGO7 fragment amplified from pBYL-AGO7 [13] using primers oligo1159 and oligo1160.
480 The two fragments were cloned into AscI-digested pBYL2 vector[12] via HiFi DNA
481 Assembly Cloning kit (New England Biolabs).

pUC57-F-TAS3_5endM_3M and pUC57-F-TAS3_5P_3M

The 5′ miR390-binding site in pUC57-F-TAS3_3M was replaced by the sequences shown in Figure 3b and Extended Data Fig. 5 by site directed mutagenesis using primer pairs oligo1101-oligo1102 and oligo 1106-oligo1107, respectively.

pUC57-TAS3_3M, pUC57-TAS3_5endM_3M, pUC57-TAS3_5P_3M, pUC57-TAS3_M(+1), pUC57-TAS3_M(+2), pUC57-TAS3_M(+3), pUC57-TAS3_M(+4), pUC57-TAS3_M(+5), pUC57-TAS3_M(+6) and pUC57-TAS3_M(+7)

The 3×FLAG tag sequences were removed from the corresponding pUC57-F-TAS3 constructs shown above by site directed mutagenesis using primers oligo1197 and oligo1198.

pUC57-TAS3_G21A_3M

The 5′ terminal G nucleotide of 5′ miR390-binding site in pUC57-TAS3_3M was substituted to A by site directed mutagenesis using primers oligo1220 and oligo1221.

pCR-Blunt II-TOPO_TAS1a

TAS1a PCR product was amplified from cDNA corresponding to *Arabidopsis* seedling total RNA using oligoA1 and oligoA2 for the TAS1a sequence and cloned into pCR Blunt II-TOPO vector (Invitrogen, #45-0245).

pCR-Blunt II-TOPO_3×FLAG-TAS1a

Three PCR fragments were prepared from pCR-Blunt II-TOPO_TAS1a: TOPO-TAS1a 5′ UTR fragment amplified with oligoA3 and oligoA4 and then digested with XhoI, FLAG-TAS1a fragment amplified with oligoA5 and oligoA6 and ORF-3′ UTR-TOPO fragment amplified with oligoA7 and oligoA8 and then digested with SpeI. To insert the 3×FLAG sequence directly in front of ORF1, the above three PCR fragments were cloned into XhoI/SpeI-digested pCR Blunt II-TOPO vector (Invitrogen) using the HiFi DNA Assembly Cloning kit (New England Biolabs).

T7-TAS1a and T7-F-Tas1a

T7-TAS1a and T7-F-Tas1a DNA templates were amplified from pCR-Blunt II-TOPO_TAS1a and pCR Blunt II-TOPO-3xFLAG-TAS1a, respectively, using a forward primer containing T7 polymerase binding site (oligoA9) and a reverse primer with poly(A) tail (oligoA10).

pAT006-TAS3a-PDS_full-length

A TAS3a fragments with a full-length 5′ UTR, a natural intron and tandem synthetic-tasiRNAs in the 5′ D7[+] and 5′ D8[+] positions (TAS3aPDS2) was synthesized via GeneArt Strings DNA Fragments service (invitrogen), gel-purified and cloned into SalI/SpeI-digested pAT006[15] vector via HiFi DNA Assembly Cloning kit (New England Biolabs).

526 *pMDC32_TAS3*

527 Two PCR products were amplified: fragment A from pAT006-TAS3a-PDS_full-length
528 using primers oligo1201 and oligo1202 and fragment B from pMDC-Tas3a[17] using
529 primers oligo1203 and oligo1204. The two fragments were cloned into KpnI/SpeI-
530 digested pMDC32 vector via HiFi DNA Assembly Cloning kit (New England Biolabs).

531

532 *pMDC32_TAS3_5M*

533 Two PCR products were amplified: fragment A from pAT006-TAS3a-PDS_full-length
534 using primers oligo1201 and oligo1209 and fragment B from pMDC-Tas3a[17] using
535 primers oligo1210 and oligo1204. The two fragments were cloned into KpnI/SpeI-
536 digested pMDC32 vector via HiFi DNA Assembly Cloning kit (New England Biolabs).

537

538 *pMDC32_early_stop*

539 Two PCR products were amplified: fragment A from pAT006-TAS3a-PDS_full-length
540 using primers oligo1201 and oligo1211 and fragment B from pMDC-Tas3a[17] using
541 primers oligo1212 and oligo1204. The two fragments were cloned into KpnI/SpeI-
542 digested pMDC32 vector via HiFi DNA Assembly Cloning kit (New England Biolabs).

543

544 *pMDC32_TAS3(+3)*

545 Two PCR products were amplified: fragment A from pAT006-TAS3a-PDS_full-length
546 using primers oligo1201 and oligo1207 and fragment B from pMDC-Tas3a[17] using
547 primers oligo1208 and oligo1204. The two fragments were cloned into KpnI/SpeI-

548 digested pMDC32 vector via HiFi DNA Assembly Cloning kit (New England Biolabs).

549

550 *pMDC32_TAS3(+6)*

551 Two PCR products were amplified: fragment A from pAT006-TAS3a-PDS_full-length
552 using primers oligo1201 and oligo1205 and fragment B from pMDC-Tas3a[17] using
553 primers oligo1206 and oligo1204. The two fragments were cloned into KpnI/SpeI-
554 digested pMDC32 vector via HiFi DNA Assembly Cloning kit (New England Biolabs).

555

556 **Production of recombinant AtSGS3 protein**

557 Recombinant AtSGS3 proteins were expressed using the Premium PLUS Expression kit
558 (Cell-Free Sciences) with pEU-6×His-SBP-SUMO-AtSGS3 according to manufacturer
559 instructions. The protein was affinity purified with streptavidin sepharose high
560 performance beads (GE Healthcare), washed three times with 1 × lysis buffer containing
561 200 mM NaCl and 0.1% TritonX-100, rinsed once with 1 × lysis buffer containing 20%
562 glycerol and 1mM DTT and eluted by 1 × lysis buffer containing 20% glycerol, 1 mM
563 DTT and 0.05 U/µl of SUMOstar protease. Protein concentration was determined using
564 SDS-PAGE with defined dilutions of BSA as concentration standards.

565

566 ***In vitro* RNA silencing assay, NuPAGE and Western blotting**

567 Typically, 7.5 µl of BY-2 lysate, 3.75 µl of substrate mixture, and 0.75 µl of 300 nM AGO
568 mRNAs were mixed and incubated at 25°C for 30 min. To assemble RISC, 1.5 µl of 1.5
569 µM miR390 or miR173 duplex was added to the reaction mixture and incubated at 25°C

570 for 90 min. Then, 1.5 µl of 100 nM TAS3a or TAS1a variant was added and further
571 incubated at 25°C for 10–60 min. For RNase treatment, 5 µl of the reaction was treated
572 with 1 µl of RNase mixture (10% RNase A, Sigma + 20% RNase One, Promega),
573 incubated at 37°C for 10 min and then mixed with 6 µl of 2 × SDS-PAGE buffer. For
574 the control, 1 µl sterile water was used instead of RNase mixture. The samples were run
575 on NuPAGE Bis-Tris Precast Gel (Thermo Fisher Scientific) at 200 V for ~30 min in 1 ×
576 NuPAGE MES SDS Buffer (Thermo Fisher Scientific) and transferred onto PVDF
577 membrane. Western blotting was performed as previously described[1] with modifications.
578 The membrane was blocked in TBST containing 1.0% nonfat dried milk (w/v) for 30 min.
579 Anti-AtSGS3 (diluted at 1:3000), anti-AtAGO7 antibodies (diluted at 1:3000), anti-
580 NtSGS3 antibody (diluted at 1:3000)[19], anti-DDDDK-tag mAb (diluted at 1:5000)
581 (Medical & Biological Laboratories) and anti-HA-tag mAb (diluted at 1:5000) (Medical
582 & Biological Laboratories) were used as primary antibodies. Peroxidase AffiniPure Goat
583 Anti-Rabbit IgG (H+L) (diluted at 1:20000) (Jackson ImmunoResearch), Anti-IgG (H+L)
584 (Mouse) pAb-HRP (diluted at 1:5000) (Medical & Biological Laboratories) and Mouse
585 TrueBlot ULTRA: Anti-Mouse Ig HRP (Rockland Immunochemicals, Inc.) (1:1000) were
586 used as secondary antibodies.
587
588 **Northern blotting**
589 For *in vitro* assays, two microliter of reaction mixture was mixed with 8 µl of low salt PK
590 solution [0.125% SDS, 12.5 mM EDTA, 12.5 mM HEPES-KOH (pH7.4) and 12.5%
591 Proteinase K (TaKaRa)], and incubated at 50°C for 10 min. Ten microliter of 2 ×

formamide dye [10 mM EDTA, pH 8.0, 98% (w/v) deionized formamide, 0.025% (w/v) xylene cyanol and 0.025% (w/v) bromophenol blue] was added into the mixture, and further incubated at 65°C for 10 minutes. For *in vivo* assays, total RNA was purified with Trizol reagent (Thermo Fisher Scientific), and 10 µl of 300–500 ng/ul total RNAs were mixed with equal volume 2 × formamide dye. Ten µl of samples were run on a denaturing 1% agarose gel, transferred to the Hybond N+ membrane with capillary blotting and fixed with UV crosslinker. For small RNAs, 10 µl of samples were run on a denaturing 18% acrylamide gel. RNAs were transferred to Hybond N membrane with electro blotting and chemically crosslinked[20]. TAS3 variants were detected with Digoxigenin (DIG)-labeled long TAS3 probe (Fig. 2d) or 5′ ^{32}P-radiolabeled oligo probe mixtures (oligo1230-1234) (Fig. 5f). F-TAS1a and its 5′ cleaved fragment were detected with a 5′ ^{32}P-radiolabeled oligo probe (oligoA4) (Fig. 4e). U6 RNA, miR173, miR390, and tasiRNAs from TAS3 variants were detected with 5′ ^{32}P-radiolabeled oligo1129, oligo1353, oligo1131, oligoD7, respectively.

Immunoprecipitation with anti-FLAG antibody

F-AGO7-RISC or F-AGO1-RISC was assembled as shown above. Target RNAs were mixed with the RISCs at a final concentration of 50 nM, and incubated for 20 min. The reaction mixture was incubated with Dynabeads protein G (Invitrogen) coated with anti-FLAG antibody on a rotator at 4°C for 1 h. The beads were washed three times with 1 × lysis buffer containing 200 mM NaCl and 1% Triton-X 100 or 1 × wash buffer (20 mM Hepes, pH 7.5, 120 mM KCl, 10 mM MgCl2 and 0.2% Nonidet P-40). After removing

buffer completely, 1×SDS-PAGE sample buffer was added to the beads. The samples (input, supernatant, and beads) were heated for 5 min and used for SDS-PAGE. Western blotting was performed as described above.

Immunodepletion of endogenous SGS3 protein

Fifty microliter of BY-2 lysate was mixed with 1.66 µg of anti-NtSGS3[19] or Normal Rabbit IgG (Medical & Biological Laboratories) at 4°C for 1h. To remove the antibodies and binding proteins thereof, the lysate was mixed with the pellet of 50 µl Dynabeads protein G, and incubated at 4°C for 1h. The supernatant was transferred into new tubes. After flash freezing by liquid nitrogen, the SGS3 or Mock-depleted lysate was stored at -80°C .

Photoactivated UV crosslinking

In vitro reaction mixtures were prepared as outlined above (*Immunoprecipitation with anti-FLAG antibody*) with F-AGO7, ^{32}P-labeled miR390_21_4SU, and TAS3-G21A-3M. The sample was transferred to Terasaki plate wells (7 µl/well) and exposed to > 300 nm UV radiation for 15 s using a UV crosslinker (SP-11 SPOT CURE, USHIO) with a uniform radiation lens (USHIO) and a long-path filter (300 nm, ASAHI SPECTRA) at 3 cm from the light. For input sample, aliquots of reaction mixture were transferred into a new tube, and mixed with 4×SDS-PAGE sample buffer. For FLAG-IP, the reaction mixture was incubated with Dynabeads protein G coated with anti-FLAG antibody on a rotator at 4°C for 1 h. For SGS3-IP, the reaction mixture was first incubated with anti-

NtSGS3 antibody at 4°C for 1 h, then with Dynabeads protein G at 4°C for another 1 h. The tube was then placed on a magnetic stand to transfer the supernatant into a new tube, which was then mixed with 4×SDS-PAGE sample buffer. The beads were washed three times with 1×lysis buffer containing 800 mM NaCl and 1% Triton-X 100. After removing the buffer completely, 1×SDS-PAGE sample buffer was added to the beads. The samples (input, supernatant, and beads) were heated for 5 min and used for SDS-PAGE. After drying, the gel was exposed to a phosphor imaging plate.

Agrobacterium-based transient expression in *Nicotiana benthamiana*

The *Nicotiana benthamiana* infiltration assay was performed as previously described[21]. Briefly, pAT006 and pMDC- plasmids were introduced into *Agrobacterium tumefaciens* GV3101 (pMP90). The *Agrobacterium* cells transformed with TAS3 constructs, AGO7, and miR390 or empty vector (pAT006) were pooled at a ratio of 1:1:2 (total optical density at 600 nm (OD600)) = 1.0). The leaves were harvested at ~48 h post-infiltration. Total RNA was extracted using Trizol reagent (Thermo Fisher Scientific).

Data availability

All sequencing data are publicly available in DDBJ, under the accession number DRA010034 (currently undisclosed). All other data are available from the authors upon reasonable request.

Methods references

1. Tomari, Y. & Iwakawa, H. O. In Vitro Analysis of ARGONAUTE-Mediated Target Cleavage and Translational Repression in Plants., *Methods Mol Biol* **1640**, 55-71 (2017).
2. Peragine, A., Yoshikawa, M., Wu, G., Albrecht, H. L. & Poethig, R. S. SGS3 and SGS2/SDE1/RDR6 are required for juvenile development and the production of trans-acting siRNAs in Arabidopsis., *Genes Dev* **18**, 2368-2379 (2004).
3. McGlincy, N. J. & Ingolia, N. T. Transcriptome-wide measurement of translation by ribosome profiling., *Methods* **126**, 112-129 (2017).
4. Kurihara, Y. et al. Transcripts from downstream alternative transcription start sites evade uORF-mediated inhibition of gene expression in Arabidopsis., *Proc Natl Acad Sci U S A* **115**, 7831-7836 (2018).
5. Kozomara, A. & Griffiths-Jones, S. miRBase: integrating microRNA annotation and deep-sequencing data., *Nucleic Acids Res* **39**, D152-7 (2011).
6. Kozomara, A. & Griffiths-Jones, S. miRBase: annotating high confidence microRNAs using deep sequencing data., *Nucleic Acids Res* **42**, D68-73 (2014).
7. Dai, X. & Zhao, P. X. psRNATarget: a plant small RNA target analysis server., *Nucleic Acids Res* **39**, W155-9 (2011).
8. Dai, X., Zhuang, Z. & Zhao, P. X. psRNATarget: a plant small RNA target analysis server (2017 release)., *Nucleic Acids Res* **46**, W49-W54 (2018).
9. Langmead, B. & Salzberg, S. L. Fast gapped-read alignment with Bowtie 2., *Nat Methods* **9**, 357-359 (2012).
10. Li, H. et al. The Sequence Alignment/Map format and SAMtools., *Bioinformatics* **25**, 2078-2079 (2009).
11. Quinlan, A. R. & Hall, I. M. BEDTools: a flexible suite of utilities for comparing genomic features., *Bioinformatics* **26**, 841-842 (2010).
12. Mine, A. et al. Identification and characterization of the 480-kilodalton template-specific RNA-dependent RNA polymerase complex of *Red clover necrotic mosaic virus*., *J Virol* **84**, 6070-6081 (2010).
13. Endo, Y., Iwakawa, H. O. & Tomari, Y. Arabidopsis ARGONAUTE7 selects miR390 through multiple checkpoints during RISC assembly., *EMBO Rep* **14**, 652-658 (2013).
14. Iwakawa, H. O. & Tomari, Y. Molecular Insights into microRNA-Mediated Translational Repression in Plants., *Mol Cell* **52**, 591-601 (2013).

15. Tsuzuki, M., Takeda, A. & Watanabe, Y. Recovery of dicer-like 1-late flowering phenotype by miR172 expressed by the noncanonical DCL4-dependent biogenesis pathway., *RNA* **20**, 1320-1327 (2014).
16. Curtis, M. D. & Grossniklaus, U. A gateway cloning vector set for high-throughput functional analysis of genes in planta., *Plant Physiol* **133**, 462-469 (2003).
17. Montgomery, T. A. et al. Specificity of ARGONAUTE7-miR390 interaction and dual functionality in TAS3 trans-acting siRNA formation., *Cell* **133**, 128-141 (2008).
18. Baeg, K., Iwakawa, H. O. & Tomari, Y. The poly(A) tail blocks RDR6 from converting self mRNAs into substrates for gene silencing., *Nat Plants* **3**, 17036 (2017).
19. Yoshikawa, M. et al. 3' fragment of miR173-programmed RISC-cleaved RNA is protected from degradation in a complex with RISC and SGS3., *Proc Natl Acad Sci U S A* **110**, 4117-4122 (2013).
20. Pall, G. S. & Hamilton, A. J. Improved northern blot method for enhanced detection of small RNA., *Nat Protoc* **3**, 1077-1084 (2008).
21. Llave, C., Kasschau, K. D. & Carrington, J. C. Virus-encoded suppressor of posttranscriptional gene silencing targets a maintenance step in the silencing pathway., *Proc Natl Acad Sci U S A* **97**, 13401-13406 (2000).

Acknowledgements

We thank James Carrington for providing *Nicotiana benthamiana* seed, *Agrobacterium tumefaciens* GV3101, pMDC32, pMDC32-3×HA-AGO7, pMDC32-TAS3a and a detailed protocol for *Agrobacterium* infiltration, Yukio Kurihara for *Arabidopsis thaliana* (Col-0) seeds, Koreaki Ito and Yuhei Chadani for helpful advice on neutral pH gel electrophoresis analyses, Yuichi Shichino and Mari Mito for technical assistance on ribosome profiling, Keisuke Shoji for kind advice and assistance on NGS data analyses, and Kyungmin Baeg and Yayoi Endo for plasmid construction. We also thank all the members of the Tomari laboratory for discussion and critical comments on the manuscript. We also thank Life Science Editors for editorial assistance. This work was supported in part by JST, PRESTO (grant JPMJPR18K2 to H.-o.I.), Grant-in-Aid for Scientific Research on Innovative Areas ('Nascent-chain Biology') (grant 26116003 to H.-o.I.), and Grant-in-Aid for Scientific Research (B) (grant 18H02380 to M.Y.). DNA libraries were sequenced by the Vincent J. Coates Genomics Sequencing Laboratory at UC Berkeley, supported by an NIH S10 OD018174 Instrumentation Grant.

Author Contributions

H.-o.I. conceived of the project and designed the experiments; H.-o.I. and T.F. performed ribosome profiling and bioinformatic analyses with the supervision of S.I; H.-o.I., A.L., and K.K. performed biochemical analyses; A.M. and A.T. performed transient expression assays in *Nicotiana benthamiana*; H.-o.I., S.I. and Y.T. wrote the manuscript with editing from all the authors; all the authors discussed the results and approved the manuscript.

Competing interests

Authors declare no competing interests.

Corresponding author

Correspondence and requests for materials should be addressed to Hiro-oki Iwakawa (iwakawa@iqb.u-tokyo.ac.jp)

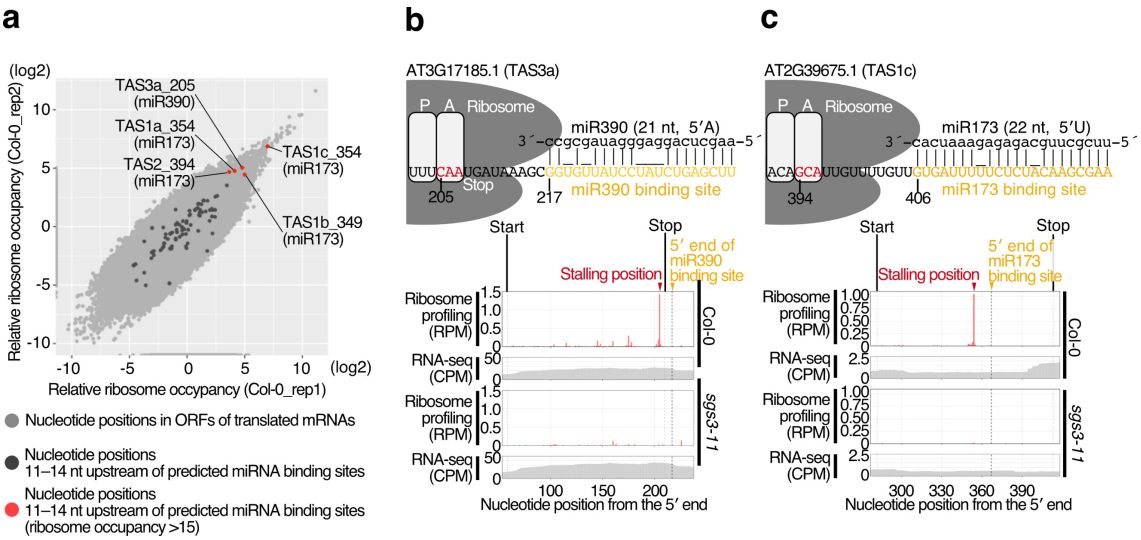

Fig. 1. The dsRNA-binding protein SGS3 promotes microRNA-mediated ribosome stalling. (a) Scatter plot showing correlation of relative ribosome occupancy (Materials and Methods) between replicates (Col-0_rep1 and 2). The nucleotide positions with ribosome footprints (reads per million (RPM) over 0.05) in translating ORFs are shown in light gray. The nucleotide positions 11–14 nucleotide upstream of predicted miRNA binding sites are shown in dark gray (Supplementary Table 1). In such positions, those with relative ribosome occupancy over 15 are shown in red (Supplementary Table 1). (b, c) Ribosome footprints (A-site position) in RPM and RNA-seq in coverage per million (CPM) in wild-type or *sgs3-11* mutant seedlings are shown for the following transcripts: (b) AT3G17185.1 (TAS3a), a precursor of trans acting siRNAs (tasiRNAs) with miR390 binding sites; (c) AT2G39675.1 (TAS1c), a precursor of tasiRNAs with a miR173 binding site. See also Extended Data Fig.1 and Supplementary Table 1.

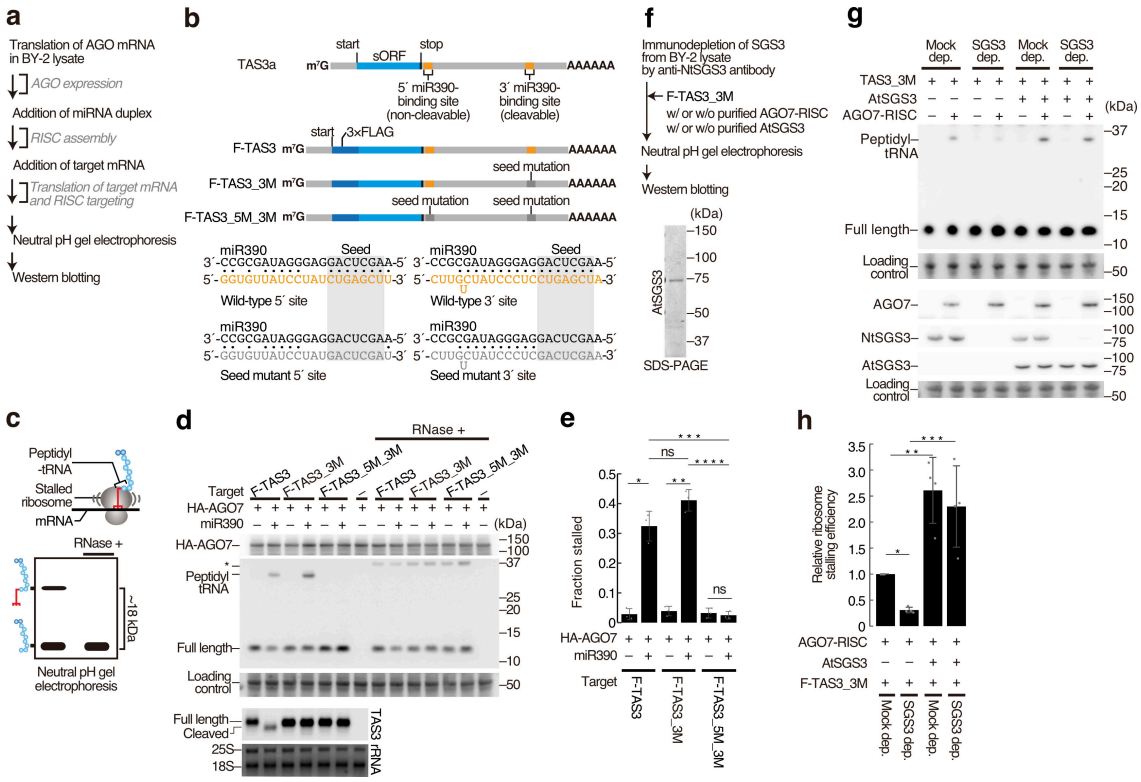

Fig. 2. *In vitro* recapitulation of microRNA-mediated ribosome stalling.
(a) Flowchart of the miRNA-mediated ribosome stalling assay *in vitro*. (b) (top) Schematic representation of TAS3a RNA and its 3×FLAG-tag fused variants. The orange and gray boxes indicate wild-type and seed-mutant miR390-binding sites, respectively. (bottom) The base-pairing configurations between miR390 and the wild-type or seed mutated miR390-binding sites. Seed sequences are shown in the shaded boxes. (c) Schematic representation of SDS-PAGE in a neutral pH environment, to thus detect peptidyl-tRNAs. (d) Both AGO7-RISC and the 5′ binding site are required for ribosome stalling *in vitro*. After *in vitro* silencing assay, half of the reaction mixture was treated with RNase (RNase +), and used for PAGE followed by Western blotting. The full-length polypeptide and peptidyl-tRNA were detected by anti-FLAG antibody. 3×HA-AGO7 (HA-AGO7) was detected by anti-HA antibody. Total protein was stained using Ponceau S, and the ~50 kDa bands were used as a loading control. The asterisk indicates the positions of the unexpected protein bands that appears with RNase treatment. (bottom) Northern blotting of TAS3 variants. Methylene blue-stained rRNA was used as a loading control. (e) Quantification of ribosome stalling efficiencies in (d). Fraction stalled was calculated using the following formula: Fraction stalled = peptidyl-tRNA/(full-length + peptidyl-tRNA). The mean values ± SD from three independent experiments are shown. Bonferroni-corrected P values from two-sided paired t-tests are as follows: *P = 0.03361; **P = 0.03817; ***P = 0.03809, ****P = 0.03174. (f) (top) Flowchart of the *in vitro* miRNA-mediated ribosome stalling assay with SGS3-immunodepleted lysate. (bottom) Coomassie brilliant blue staining of purified AtSGS3. (g) SGS3 promotes miRNA-mediated ribosome stalling *in vitro*. Endogenous NtSGS3, recombinant AtSGS3, and recombinant AGO7 were detected using anti-NtSGS3, anti-AtSGS3, and anti-AtAGO7 antibodies, respectively. See also Fig. 2d legend. (h) Quantification of relative ribosome stalling efficiencies in (g). The signal intensity of peptidyl-tRNA/(full-length + peptidyl-tRNA) was normalized to the value of Mock dep. (AtSGS3 –). The mean values ± SD from four independent experiments are shown. Bonferroni-corrected P values from two-sided paired t-tests are as follows: *P = 0.00039; **P = 0.04433; ***P = 0.03889.

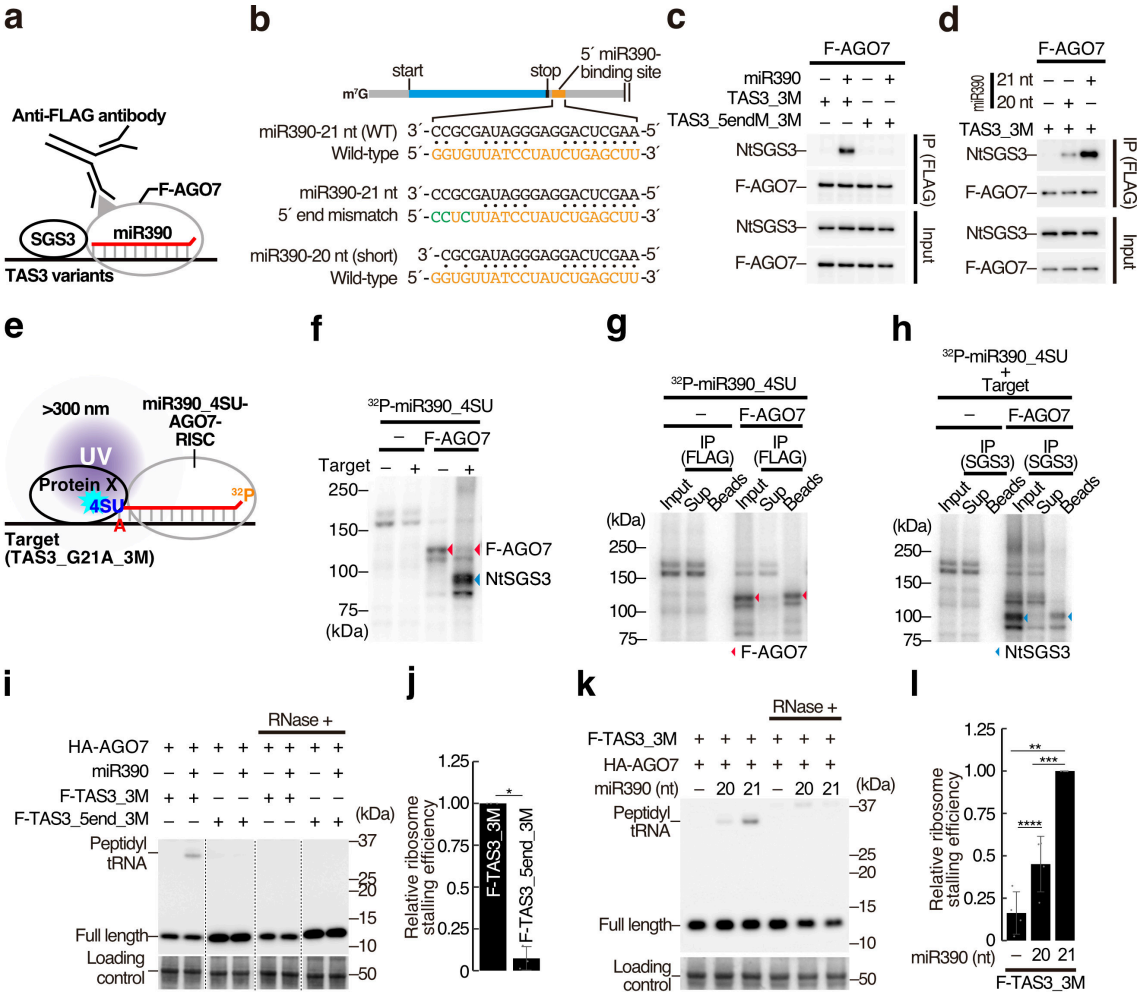

Fig. 3. SGS3 binding to the 3′ end of miR390 is required for the ribosome pausing.
(a) Schematic representation of co-immunoprecipitation assay with anti-FLAG antibody in the presence of F-AGO7, miR390, and TAS3 variants. (b) Base-pairing configurations. (top) miR390 and wild-type 5′ miR390-binding site. (middle) miR390 and 5′ site with 5′ end mismatches (5endM). (bottom) 20-nt miR390 and the wild-type 5′ site. The mutated nucleotides are shown in green. (c) 5′ end mismatches in the 5′ site disrupt interaction between SGS3 and AGO7. (d) The use of a short miR390 variant (20 nt) disrupted interaction between SGS3 and AGO7. (e) An overview of the UV crosslink experiment. AGO7 was programmed with the 5′-radiolabeled miR390 variant bearing the 3′ 4-thio-U (^{32}P-miR390_4SU) in BY-2 lysate, and further incubated with the TAS3 variant (TAS3_G21A_3M). The reaction mixture was analyzed using 10% SDS-PAGE and crosslinked proteins were detected using phosphorimaging. The ellipse indicates neighboring proteins. (f) miR390-loaded AGO7 directly interacts with NtSGS3 in the presence of TAS3_G21A_3M. 5′ end-radiolabeled miR390 with a 3′ 4-thio-U was incubated in BY-2 lysate in the presence or absence of F-AGO7 and target RNA (TAS3_G21A_3M), crosslinked by UV light (>300 nm), then analyzed by SDS-PAGE. The red and blue arrowheads indicate AGO7 and NtSGS3, respectively (See also g and h). (g) Detection of F-AGO7 by UV crosslinking. The 5′ end-radiolabeled miR390 with a 3′ 4-thio-U was incubated in BY-2 lysate in the presence of F-AGO7, crosslinked by UV light (>300 nm), immunoprecipitated using anti-FLAG antibody, and then analyzed by SDS-PAGE. F-AGO7 was efficiently crosslinked to 4-thio-U at the 3′ end of miR390. (h) Detection of NtSGS3 by UV crosslinking. 5′ end-radiolabeled miR390 with a 3′ 4-thio-U was incubated in BY-2 lysate in the presence of F-AGO7 and target RNA (TAS3_G21A_3M), crosslinked by UV light (>300 nm),

805 immunoprecipitated by anti-NtSGS3 antibody, and then analyzed by SDS-PAGE. NtSGS3 was
806 efficiently crosslinked to 4-thio-U at the 3′ end of miR390 in the presence of the target RNA. (i) and
807 (k) *in vitro* ribosome stalling experiments. Mismatches at the 5′ end of miR390-binding site or the use
808 of 20-nt miR390 decreased stalled ribosomes. See also the legend of Fig.2d. (j) and (l) Quantification
809 of relative ribosome stalling efficiencies in (i) and (k), respectively. The signal intensity of peptidyl-
810 tRNA/(full-length + peptidyl-tRNA) was normalized to the value of F-TAS3_3M (i) or miR390 (21
811 nt) (k). The mean values ± SD from three (j) and four (l) independent experiments are shown,
812 respectively. P value from two-sided paired t-tests are as follows: *P = 0.00190 (j). Bonferroni-
813 corrected P values from two-sided paired t-tests are as follows: **P = 0.00270; ***P = 0.02034; ****P
814 = 0.04343 (l).
815

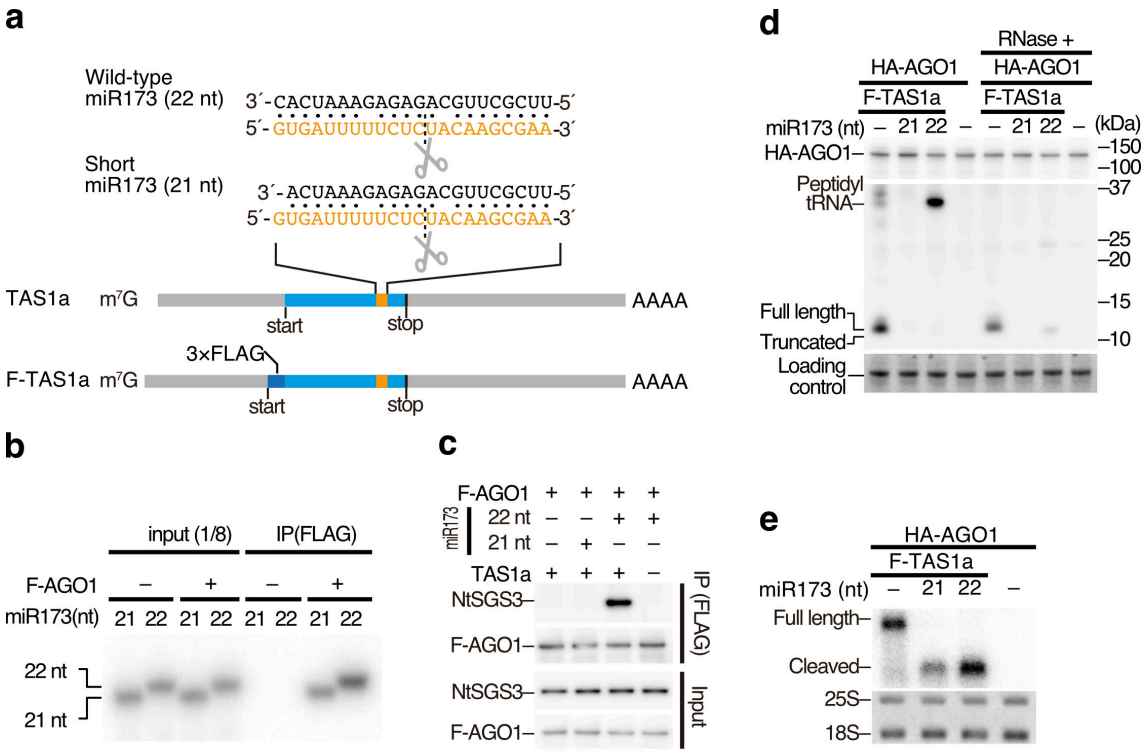

Fig. 4. AGO1 loaded with 22-nt miR173 efficiently stalls ribosome. (a) (top) Base-pairing configurations between 22/21-nt miR173 and the miR173-binding site in TAS1a. (bottom) Schematic representation of TAS1a RNA and its 3×FLAG-tag fused variant. (b) *In vitro* RISC assembly with AGO1 and radiolabeled 21 and 22-nt miR173 duplexes. After translation of 3×FLAG-AGO1 (F-AGO1) mRNA *in vitro*, the radiolabeled miR173 duplex was added and further incubated for RISC assembly. Then, F-AGO1 was immunoprecipitated with anti-FLAG antibody. The co-immunoprecipitated miR173 was analyzed by denaturing PAGE. Both 21- and 22-nt miR173 duplexes were incorporated into AGO1. (c) Co-immunoprecipitation experiments with 3×FLAG-AGO1 in the presence of 21 or 22-nt miR173 duplex and TAS1a RNA. AGO1-RISC loaded with 22-nt miR173 interacts with NtSGS3 in the presence of TAS1a RNA. In contrast, 21-nt miR173 failed to promote the interaction between AGO1 and NtSGS3. (d) *In vitro* ribosome stalling experiments. Peptidyl-tRNA was accumulated in the presence of AGO1-RISC loaded with 22-nt miR173, while no peptidyl-tRNA was observed in the presence of that with 21-nt miR173. (e) Northern blotting of TAS1 reporter RNAs. TAS1 was efficiently cleaved by AGO1-RISC loaded with 21- and 22-nt miR173. Methylene blue-stained rRNA was used as a loading control.

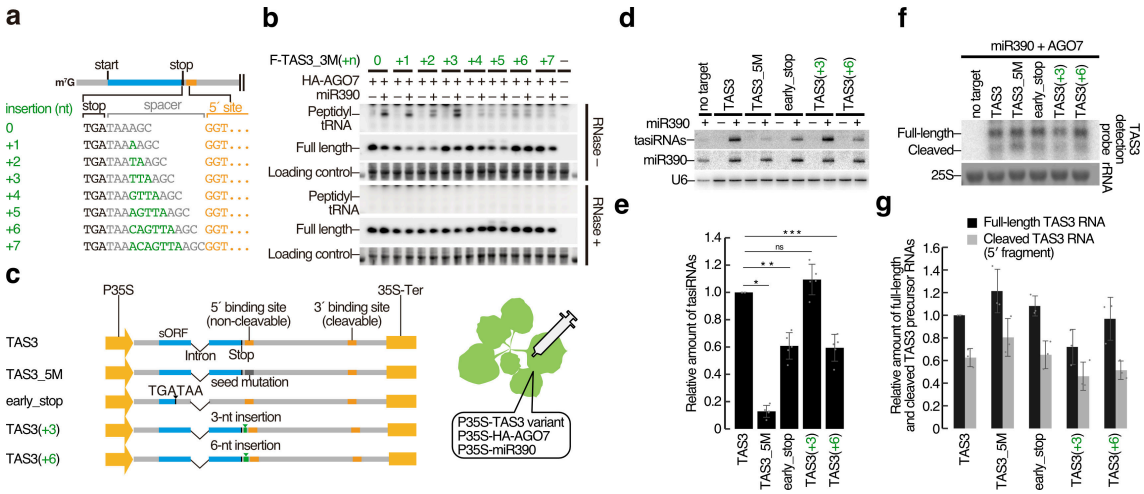

Fig. 5. Ribosome stalling enhances production of secondary siRNAs.

(a) Schematic representation of TAS3 variants with different nucleotide insertions (green) between the stop codon (black) and the 5′ miR390-binding site (orange). (b) *In vitro* ribosome stalling experiments. Insertions of over 3 nucleotides decreased stalled ribosomes. After *in vitro* silencing assay, half of the reaction mixture was treated with RNase (RNase +), and used for PAGE followed by Western blotting. The full-length polypeptide and peptidyl-tRNA were detected by anti-FLAG antibody. Total protein was stained using Ponceau S, and the ~50 kDa bands were used as a loading control. (c) Schematic representation of plasmids carrying TAS3 variants used in the *Nicotiana benthamiana (N. benthamiana)* transient assay. P35S and 35S-Ter indicate Cauliflower mosaic virus (CaMV) 35S promoter and terminator, respectively. Leaves of *N. benthamiana* plants were infiltrated with a mixture of *Agrobacterium tumefaciens* cultures harboring P35S-HA-AGO7, P35S-TAS3 variants, and P35S-miR390 or empty vector. Leaves were harvested at 2-day post infiltration and used for Northern blotting to detect secondary siRNAs and the sense strand of TAS3 mRNAs. (d) Northern blotting of secondary siRNAs from TAS3 and its variants, miR390, and U6 RNAs. (e) Quantification of the secondary siRNAs in (d). The signal intensity of tasiRNAs was calibrated with miR390, and normalized to the value of TAS3 (miR390 +). The mean values ± SD from five independent experiments are shown. Bonferroni-corrected P values from two-sided paired t-tests are as follows: *P = 5.96313E-06; **P = 0.00332; ***P = 0.00329. A positive correlation was observed between tasiRNA biogenesis and miR390-mediated ribosome stalling. (f) Northern blotting of the full-length TAS3 RNAs and the 5′ cleaved fragments. Methylene blue-stained rRNA was used as a loading control. (g) The signal intensity of TAS3 RNA/rRNA was normalized to the value of full-length TAS3. The mean values ± SD from three independent experiments are shown. No correlation was observed between ribosome stalling and accumulation of the sense strand of TAS3 RNAs.

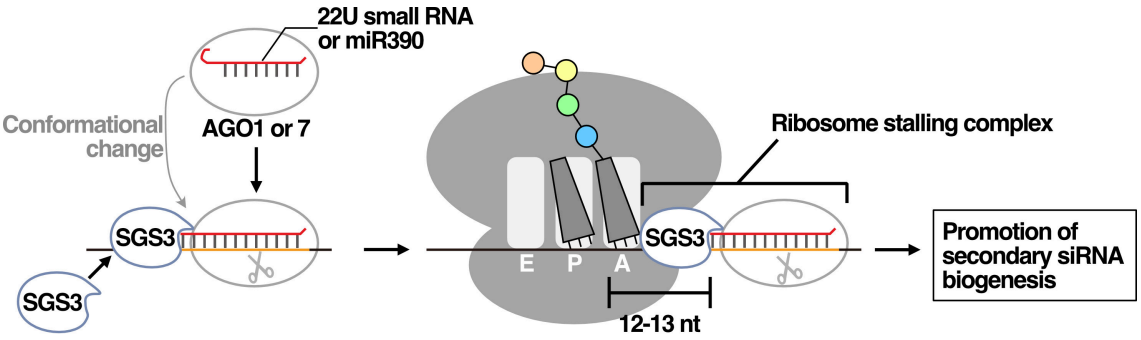

Fig. 6. A model for ribosome stalling caused by SGS3-miRNA-Argonaute complex and its role in secondary siRNA biogenesis.

Target binding causes dynamic conformational changes in 22U-AGO1-RISC or miR390-AGO7-RISC, resulting in protrusion of the 3′ end of the small RNA from the RISC complex. SGS3 directly binds the dsRNA formed between the 3′ side of the small RNA and the 5′ side of the target site. The SGS3-small RNA complex stalls ribosomes at 12–13 nt upstream of the binding sites. This ribosome stalling stimulates secondary siRNA production in a manner different from mRNA stabilization.

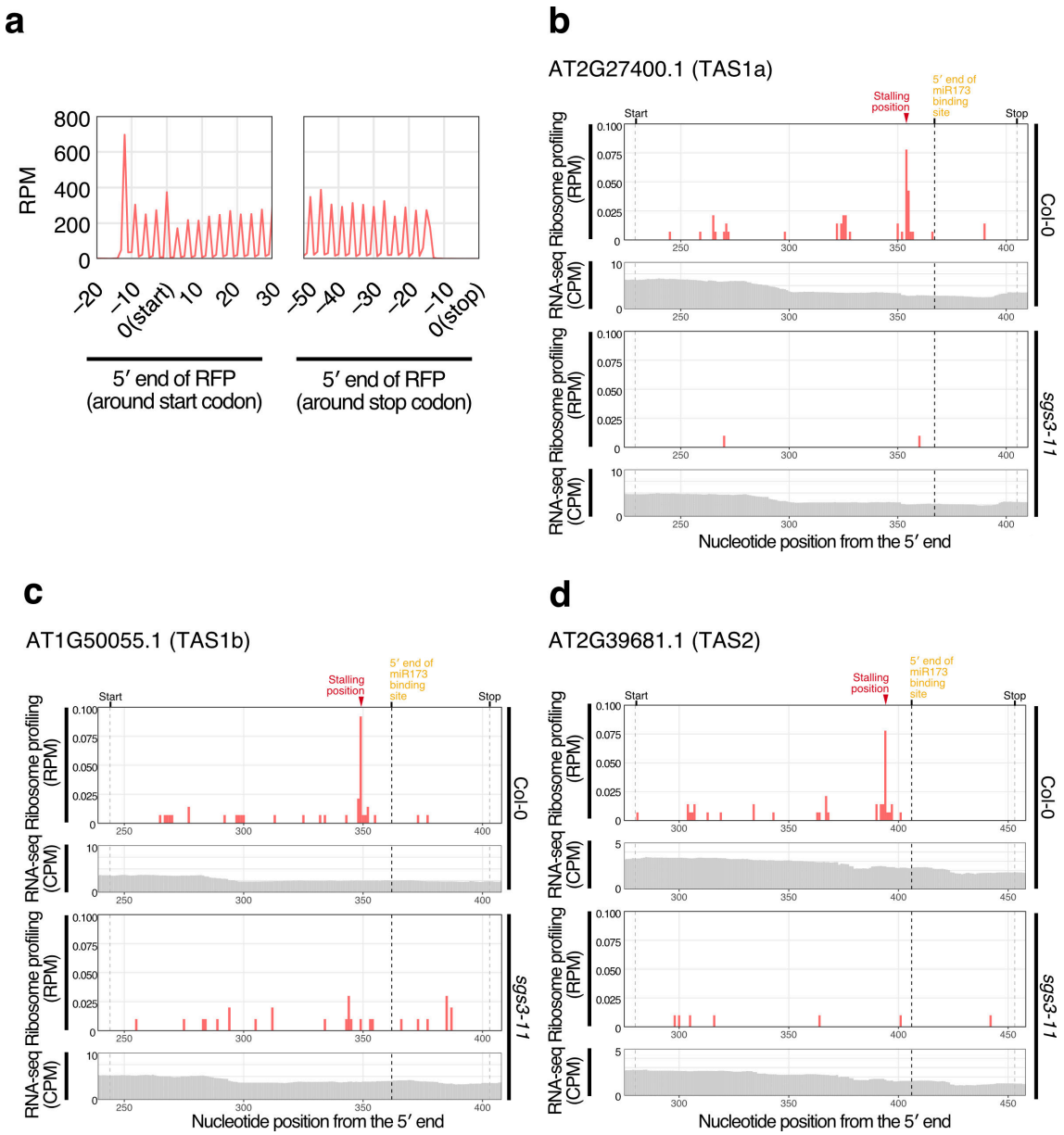

Extended Data Fig. 1. Representative ribosome stalling positions with a downstream miRNA-binding site. (a) Ribosome occupancies around start (left) and stop (right) codons using 28 nt foot prints for 3 day old seedlings of wild-type *Arabidopsis thaliana* (Col-0). The traces indicate 5′ end of ribosome footprints. Ribosome footprints (A-site positions) in RPM and RNA-seq in CPM in 3 day old wild-type or *sgs3-11* mutant seedlings are shown for the following transcripts: (b) AT2G27400.1 (TAS1a), encoding one of the isoforms of TAS1; (c) AT1G50055.1 (TAS1b) encoding one of the isoforms of TAS1; (d) AT2G39681.1 (TAS2) encoding a precursor of tasiRNAs with a miR173 binding site. Related to Figs. 1b and c.

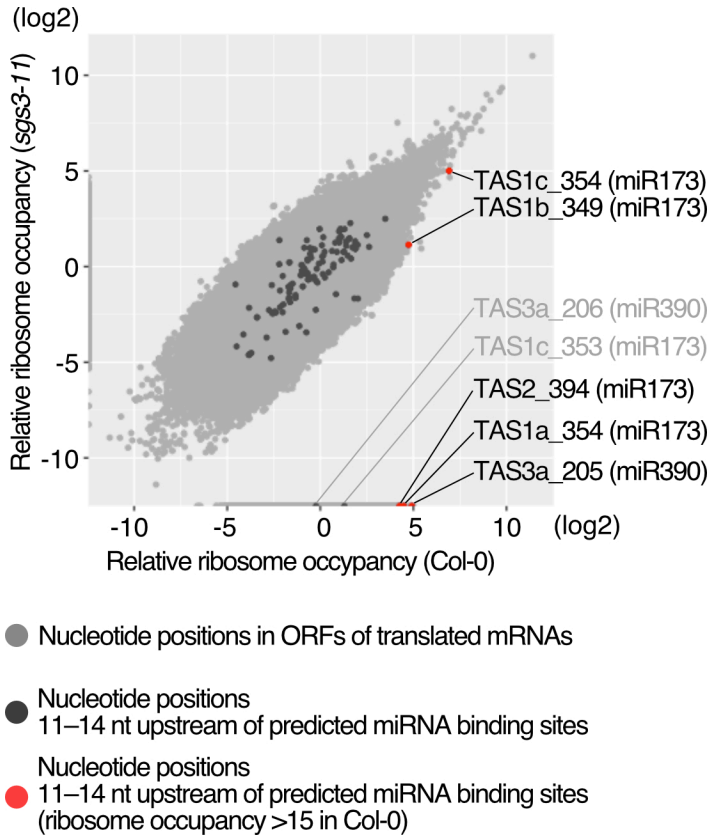

Extended Data Fig. 2. SGS3 is not a general ribosome stalling factor, but rather a specific stalling enhancer for miRNA-mediated ribosome stalling.
A scatter plot shows the relative ribosome occupancy (Materials and Methods) between Col-0 and *sgs3-11* seedlings. The nucleotide positions with ribosome footprints (RPM over 0.05 in Col-0 or *sgs3-11*) in translating ORFs are shown in light gray. See also the legend of Fig. 1a.

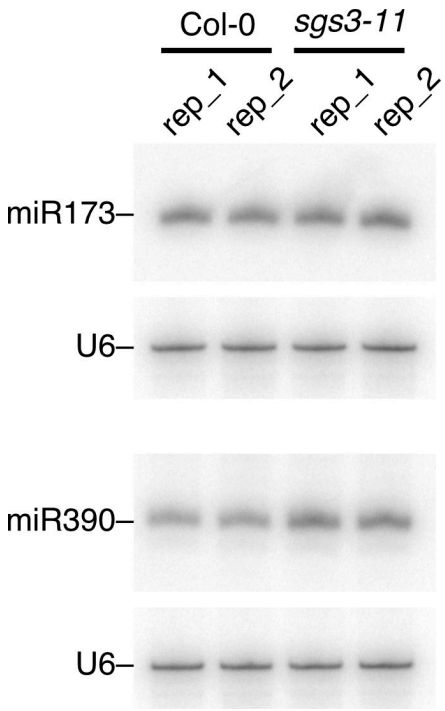

Extended Data Fig. 3. miR173 and miR390 abundance in Col-0 and *sgs3-11* seedlings.

miR173 and miR390 in wild-type (Col-0) and *sgs3-11* seedlings were detected by Northern blotting. U6 RNA was used as a loading control.

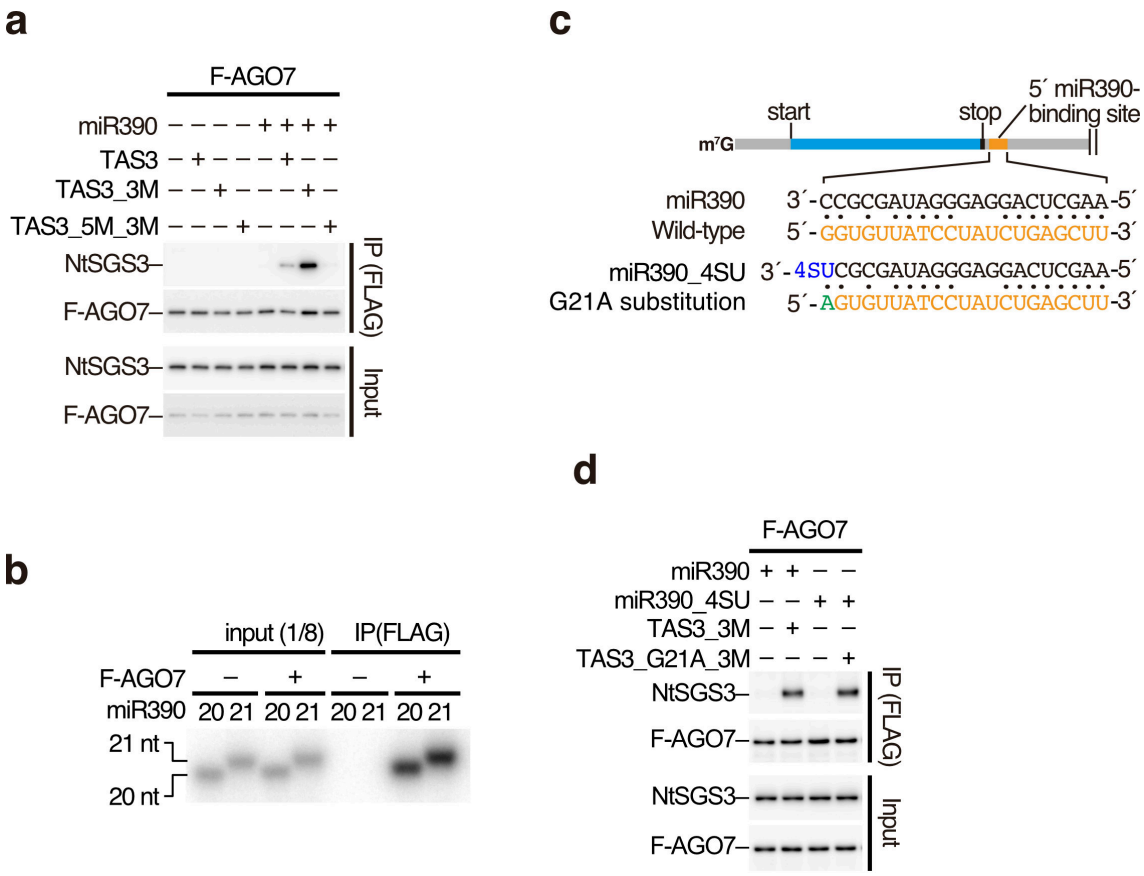

Extended Data Fig. 4. Co-immunoprecipitation of NtSGS3 with AGO7 in the presence of TAS3 variants, and AGO7-RISC assembly with 21-nt and 20-nt miR390. (a) NtSGS3 was specifically co-immunoprecipitated with F-AGO7 in the presence of miR390 duplex and TAS3 or the TAS3-3M. The reason why more SGS3 was co-immunoprecipitated in TAS3_3M than wild-type TAS3 is because the wild-type TAS3 mRNA is cleaved at the 3′ binding site by AGO7-RISC, thereby destabilized in the lysate as shown in Fig. 2d. (b) *In vitro* RISC assembly with F-AGO7 and radiolabeled 20 and 21-nt miR390 duplexes. After RISC assembly, F-AGO7 was immunoprecipitated with anti-FLAG antibody. The co-immunoprecipitated miR390 was analyzed by denaturing PAGE. Both 20- and 21-nt miR390 duplexes were efficiently incorporated into AGO7. (c) Schematic of base-pairing configurations between miR390-4SU and a 5′ miR390-binding site with a G21A substitution. The mutated nucleotides in TAS3 variant are shown in green. 4-thiouridine is shown in blue. (d) AGO7-RISC loaded with 21-nt miR390 variant possessing 4-thiouridine at the 3′ end (miR390_4SU) efficiently interacts with NtSGS3 in the presence of TAS3 variant with a compensatory G-to-A mutation at the 5′ end of miR390 binding site (TAS3_G21A_3M).

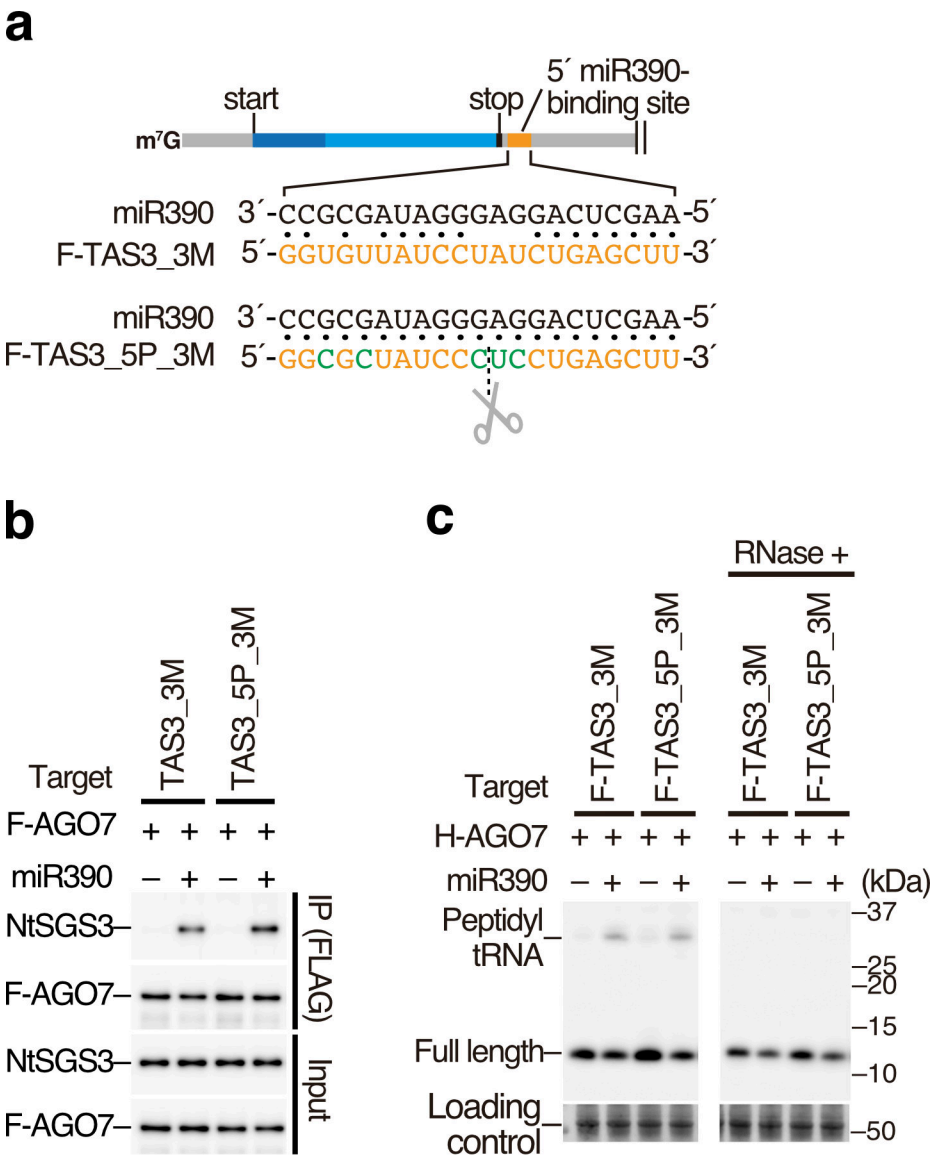

Extended Data Fig. 5. A cleavable target site facilitates ribosome stalling mediated by the miR390-AGO7 RISC. (a) Schematic of base-pairing configurations between miR390 and a 5′ target site with perfect complementarity to miR390. The mutated nucleotides in the TAS3 variant (F-TAS3_5P_3M) are shown in green. (b) Co-immunoprecipitation experiments. AGO7-RISC efficiently interacts with SGS3 in the presence of a F-TAS3_3M variant with a 5′ target site with perfect complementarity to miR390 (F-TAS3_5P_3M). (d) *In vitro* ribosome stalling experiments. Peptidyl-tRNA was accumulated in the presence of AGO7-RISC and F-TAS3_5P_3M, suggesting that cleavable site facilitates ribosome stalling mediated by miR390-AGO7-RISC.

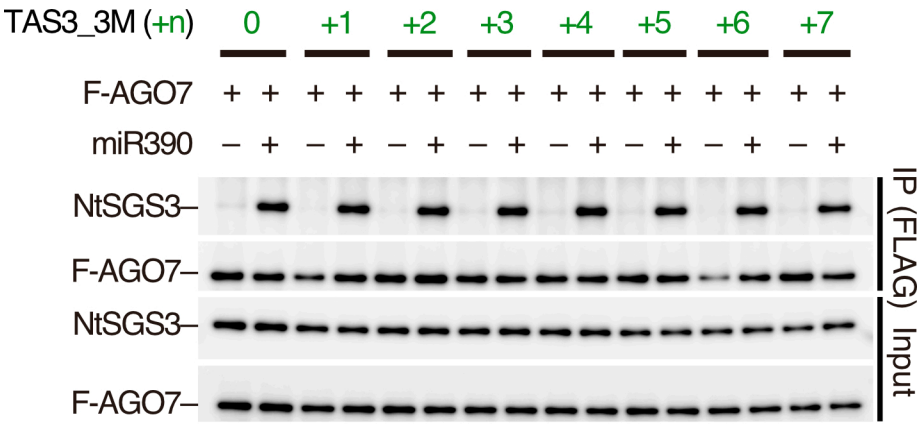

Extended Data Fig. 6. Nucleotide insertion between the stop codon and the 5′ miR390 binding site has no effect on the interaction between AGO7 and NtSGS3. NtSGS3 was specifically and efficiently co-immunoprecipitated with F-AGO7 in the presence of miR390 duplex and TAS3 variants with nucleotide insertions between the stop codon and the 5′ miR390-binding site.

Supplementary Table 1. Nucleotide positions 11–14 nt upstream of predicted miRNA binding sites.

Supplementary Table 2. List of TAS3 homologs.

Supplementary Table 3. List of synthetic RNA oligos used in this study.

Supplementary Table 4. List of synthetic DNA oligos and long DNA fragments used in this study.

Supplementary Table 1. Nucleotide positions 11–14 nt upstream of predicted miRNA binding sites.

ID	Acc.	A_site	Occupancy_Col-0_rep	Occupancy_Col-0_r	Occupancy_Col-0	Occupancy_*sgs3-11*_rep	Occupancy_*sgs3-11*_rep	Occupancy_*sgs3*	miRNA_Acc.	Expectation	miRNA_start	miRNA_end	Target_start	Target_end	miRNA_aligned_fragment	Target_aligned_fragment	Target_Desc.	distance_A_site_target_site	occupancy_ratio (*sgs3-11*/Col-0)
AT2G39675.1_354	AT2G39675.1	354	124.9047619	116.90625	120.905506	21.5	43	32.25	ath-miR173-5p	1.5	1	22	367	388	UUCGCUUGCAGAGAGAAAUCAC	GUGAUUUUUCUCUACAAGCGAA	| Symbols: TAS1C | TAS1C; other RN	13	0.266737232
AT3G17185.1_205	AT3G17185.1	205	27.38095238	32.93413174	30.15754206	0	0	0	ath-miR390a	3	1	21	217	237	AAGCUCAGGAGGGAUAGCGCC	GGUGUUAUCCUAUCUGAGCUU	| Symbols: TASIR-ARF, TAS3, ATT	12	0
AT1G50055.1_349	AT1G50055.1	349	31.8	21.82352941	26.81176471	0	4.416666667	2.208333333	ath-miR173-5p	2.5	1	22	362	383	UUCGCUUGCAGAGAGAAAUCAC	GUGAUUUUUCUCAACAAGCGAA	| Symbols: TAS1B | TAS1B; other RN	13	0.082364341
AT2G27400.1_354	AT2G27400.1	354	17.4	27.29411765	22.34705882	0	0	0	ath-miR173-5p	1.5	1	22	367	388	UUCGCUUGCAGAGAGAAAUCAC	GUGAUUUUUCUCUACAAGCGAA	| Symbols: TAS1A | TAS1A; other R	13	0
AT2G39681.1_394	AT2G39681.1	394	12.66666667	25.65	19.15833333	0	0	0	ath-miR173-5p	1.5	1	22	406	427	UUCGCUUGCAGAGAGAAAUCAC	GUGAUUUUUCUCUCCAAGCGAA	| Symbols: TAS2 | TAS2; other RNA	12	0
AT4G37150.1_725	AT4G37150.1	725	10.92266667	11.55234657	11.23750662	4.48	6.826666667	5.653333333	ath-miR5595a	1	1	21	738	758	ACAUAUGAUCUGCAUCUUUGC	UCAAAGAUGCAGAUCAUAUGC	| Symbols: ATMES9, MES9 | methyl	13	0.503077197
AT3G10160.1_778	AT3G10160.1	778	6.12745098	6.188118812	6.157784896	4.08496732	0	2.04248366	ath-miR865-3p	2.5	1	21	790	810	UUUUUCCUCAAAUUUAUCCAA	UUGGAUAUAUCUGAGGAAAAG	| Symbols: ATDFC, DFC, FPGS2 | D	12	0.331691297
AT1G52070.1_340	AT1G52070.1	340	5.461956522	5.878940731	5.670448627	2.70723593	3.540372671	3.1238043	ath-miR846	2.5	1	21	354	374	UUGAAUUGAAGUGCUUGAAUU	GAUGCAAGCACUUGAAUUCAA	| Symbols: | Mannose-binding lectin s	14	0.550891915
AT2G36400.1_732	AT2G36400.1	732	5.420233463	2.685560054	4.052896759	0.627760252	0	0.313880126	ath-miR396a	3	1	21	746	767	UUCCACA-GCUUUCUUGAACUG	CCGUUCAAGAAAGCCUGUGGAA	| Symbols: AtGRF3, GRF3 | growth-r	14	0.077445873
AT1G19540.1_598	AT1G19540.1	598	3.415977961	4.626865672	4.021421817	3.315508021	1.09540636	2.205457191	ath-miR868-3p	3	1	21	609	629	CUUCUUAAGUGCUGAUAAUGC	CCAUUGUCAACACUGAAGAAG	| Symbols: | NmrA-like negative trans	11	0.548427221
AT1G60430.1_361	AT1G60430.1	361	2.676923077	4.68161435	3.679268713	3.824175824	0	1.912087912	ath-miR5020b	2	1	21	375	395	AUGGCAUGAAAGAAGGUGAGA	AAUCACCUUCUUUCGUGCUAA	| Symbols: ARPC3 | actin-related prot	14	0.519692379
AT1G60430.1_361	AT1G60430.1	361	2.676923077	4.68161435	3.679268713	3.824175824	0	1.912087912	ath-miR5020c	2.5	1	21	374	394	UGGCAUGGAAGAAGGUGAGAC	CAAUCACCUUCUUUCGUGCUA	| Symbols: ARPC3 | actin-related prot	13	0.519692379
AT1G60430.2_394	AT1G60430.2	394	2.676923077	4.68161435	3.679268713	3.824175824	0	1.912087912	ath-miR5020b	2	1	21	408	428	AUGGCAUGAAAGAAGGUGAGA	AAUCACCUUCUUUCGUGCUAA	| Symbols: ARPC3 | actin-related prot	14	0.519692379
AT1G60430.2_394	AT1G60430.2	394	2.676923077	4.68161435	3.679268713	3.824175824	0	1.912087912	ath-miR5020c	2.5	1	21	407	427	UGGCAUGGAAGAAGGUGAGAC	CAAUCACCUUCUUUCGUGCUA	| Symbols: ARPC3 | actin-related prot	13	0.519692379
AT4G29950.2_980	AT4G29950.2	980	4.439150402	2.883511075	3.661330738	3.175607002	1.331439394	2.253523198	ath-miR5634	3	1	21	991	1011	AGGGACUUUGUGAAUUUAGGG	CUUUGAAUUCAAAAAGUUUCU	| Symbols: | Ypt/Rab-GAP domain of	11	0.615492934
AT5G03455.1_268	AT5G03455.1	268	4.626760563	2.678899083	3.652829823	3.804560261	1.201646091	2.503103176	ath-miR5646	3	1	20	281	300	GUUCGAGGCACGUUGGGAGG	UCUUCCAUUGUGCCUUGAGC	| Symbols: CDC25, ARATH;CDC25	13	0.685250421
AT4G37150.1_724	AT4G37150.1	724	5.347258486	1.780869565	3.564064025	0.630541872	0	0.315270936	ath-miR5595a	1	1	21	738	758	ACAUAUGAUCUGCAUCUUUGC	UCAAAGAUGCAGAUCAUAUGC	| Symbols: ATMES9, MES9 | methyl	14	0.088458269
AT4G29950.1_987	AT4G29950.1	987	3.94627383	2.670106417	3.308190124	2.825938567	1.171145686	1.998542126	ath-miR5634	3	1	21	998	1018	AGGGACUUUGUGAAUUUAGGG	CUUUGAAUUCAAAAAGUUUCU	| Symbols: | Ypt/Rab-GAP domain of	11	0.604119489
AT5G04200.1_1079	AT5G04200.1	1079	4.452054795	1.829268293	3.140661544	0	2.671232877	1.335616438	ath-miR5029	3	1	21	1092	1112	AAUGAGAGAGAACACUGCAAA	UUUGCGUUGUUUUCUUUUAUU	| Symbols: AtMC9, MC9 | metacaspa	13	0.425265957
AT4G34090.3_493	AT4G34090.3	493	2.356495468	3.754512635	3.055504052	3.842364532	5.811258278	4.826811405	ath-miR5636	3	1	21	505	525	CGUAGUUGCAGAGCUUGACGG	UCGUCAGGCUCUGUUACUGCG	| Symbols: | unknown protein; FUNC	12	1.57971036
AT3G51270.2_333	AT3G51270.2	333	1.982683983	3.920114123	2.951399053	2.726190476	2.871473354	2.798831915	ath-miR5631	2.5	1	21	346	366	UGGCAGGAAAGACAUAAUUUU	UGGGUUAUGACUUUCUUGCCA	| Symbols: | protein serine/threonine k	13	0.948306842
AT3G51270.1_307	AT3G51270.1	307	1.941052632	3.794238683	2.867645657	2.609433962	2.777108434	2.693271198	ath-miR5631	2.5	1	21	320	340	UGGCAGGAAAGACAUAAUUUU	UGGGUUAUGACUUUCUUGCCA	| Symbols: | protein serine/threonine k	13	0.939192467
AT3G17185.1_204	AT3G17185.1	204	3.06122449	2.462121212	2.761672851	1.818181818	1.162790698	1.490486258	ath-miR390a	3	1	21	217	237	AAGCUCAGGAGGGAUAGCGCC	GGUGUUAUCCUAUCUGAGCUU	| Symbols: TASIR-ARF, TAS3, ATT	13	0.539704135
AT1G77330.1_628	AT1G77330.1	628	3.857354028	1.407795611	2.632574819	2.196644461	2.768179174	2.482411817	ath-miR3933	2.5	1	21	639	659	AGAAGCAAAAUGACGACUCGG	AGGAGGUGUCGUUUUGCUUUU	| Symbols: | 2-oxoglutarate (2OG) and	11	0.942959645
AT1G52060.1_340	AT1G52060.1	340	4.577259475	0.667375133	2.622317304	2.13787234	2.128813559	2.13334295	ath-miR846	2.5	1	21	354	374	UUGAAUUGAAGUGCUUGAAUU	GAUGCAAGCACUUGAAUUCAA	| Symbols: | Mannose-binding lectin s	14	0.813533491
AT4G34090.1_296	AT4G34090.1	296	1.914430747	3.018867925	2.466649336	3.06738962	4.721780604	3.894585112	ath-miR5636	3	1	21	308	328	CGUAGUUGCAGAGCUUGACGG	UCGUCAGGCUCUGUUACUGCG	| Symbols: | unknown protein; FUNC	12	1.57889695
AT2G39675.1_353	AT2G39675.1	353	2.205128205	2.6875	2.446314103		0	0	ath-miR173-5p	1.5	1	22	367	388	UUCGCUUGCAGAGAGAAAUCAC	GUGAUUUUUCUCUACAAGCGAA	| Symbols: TAS1C | TAS1C; other RN	14	0
AT1G76160.1_354	AT1G76160.1	354	2.466679658	2.348769899	2.407784778	1.839654721	1.610718273	1.725186497	ath-miR4221	1.5	1	22	366	387	UUUUCCUCUGUUGAAUUCUUGC	AAUGGAAUUCAACAGAGGAGGA	| Symbols: sks5 | SKU5 similar 5 | chr	12	0.716503615
AT2G25980.1_306	AT2G25980.1	306	1.788844622	2.951789627	2.370317124	0.984649123	2.403211418	1.693930271	ath-miR846	1.5	1	21	317	337	UUGAAUUGAAGUGCUUGAAUU	GAUCCAAGCACUUCAAUUCGA	| Symbols: | Mannose-binding lectin s	11	0.714642886
AT4G25210.1_566	AT4G25210.1	566	2.104575163	2.301438399	2.203006781	2.042553191	0.493297587	1.267925389	ath-miR864-3p	2	1	22	578	599	UAAAGUCAAUAAUACCUUGAAG	CUUCAAGGUAUUAUUGAUUUCA	| Symbols: | DNA-binding storekeeper	12	0.575543117
AT1G48410.2_498	AT1G48410.2	498	1.603753	2.694775435	2.149264218	1.140808344	4.707112971	2.923960657	ath-miR168a	3	1	21	511	531	UCGCUUGGUGCAGGUCGGGAA	UUCCCGAGCUGCAUCAAGCUA	| Symbols: AGO1 | Stabilizer of iron t	13	1.360447279
AT1G48410.3_508	AT1G48410.3	508	1.603753	2.694775435	2.149264218	1.140808344	4.707112971	2.923960657	ath-miR168a	3	1	21	521	541	UCGCUUGGUGCAGGUCGGGAA	UUCCCGAGCUGCAUCAAGCUA	| Symbols: AGO1 | Stabilizer of iron t	13	1.360447279
AT1G48410.1_498	AT1G48410.1	498	1.603497268	2.688656771	2.146077019	1.14235884	4.702363147	2.922360994	ath-miR168a	3	1	21	511	531	UCGCUUGGUGCAGGUCGGGAA	UUCCCGAGCUGCAUCAAGCUA	| Symbols: AGO1 | Stabilizer of iron t	13	1.361722327
AT2G38770.1_3161	AT2G38770.1	3161	1.185388845	3.04233871	2.113863777	3.150313152	4.715625	3.932969076	ath-miR1886.2	3	1	21	3173	3193	UGAGAUGAAAUCUUUGAUUGG	CCGUUCAAAGAUUUCUUCUCA	| Symbols: EMB2765 | P-loop contain	12	1.860559379
AT5G20580.1_1170	AT5G20580.1	1170	2.468085106	1.714285714	2.09118541	2.11550152	5.272727273	3.694114396	ath-miR394a	3	1	20	1184	1203	UUGGCAUUCUGUCCACCUCC	GGAGGUGGAGAGAAUAUCAA	| Symbols: | BEST Arabidopsis thaliar	14	1.766516913
AT2G44620.1_103	AT2G44620.1	103	2.157655382	1.91840204	2.038028711	2.504757136	2.296470588	2.400613862	ath-miR869.1	3	1	21	116	136	AUUGGUUCAAUUCUGGUGUUG	AAACCCUAGGAUUGAAUCAGU	| Symbols: MTACP-1, MTACP1 | mi	13	1.177909737
AT5G20580.2_1170	AT5G20580.2	1170	2.391752577	1.629976581	2.010864579	2.005763689	5.155555556	3.580659622	ath-miR394a	3	1	20	1184	1203	UUGGCAUUCUGUCCACCUCC	GGAGGUGGAGAGAAUAUCAA	| Symbols: | BEST Arabidopsis thaliar	14	1.780656768
AT3G22890.1_430	AT3G22890.1	430	2.044714325	1.964035411	2.004374868	3.519797276	2.04415011	2.781973693	ath-miR395a	3	1	21	442	462	CUGAAGUGUUUGGGGGAACUC	GAGUUCCUCCAAACUCUUCAU	| Symbols: APS1 | ATP sulfurylase 1	12	1.387950796
AT1G23390.1_518	AT1G23390.1	518	1.15542522	2.563673545	1.859549383	2.18466731	1.214977974	1.699822642	ath-miR775	3	1	20	531	550	UUCGAUGUCUAGCAGUGCCA	UGGAGCUGUUCGACAUCGAA	| Symbols: | Kelch repeat-containing F	13	0.914104598
AT2G39700.1_736	AT2G39700.1	736	3.347322721	0.235779817	1.791551269	0.463480613	0.273404255	0.368442434	ath-miR865-3p	3	1	21	747	767	UUUUUCCUCAAAUUUAUCCAA	UUGGAUGAGUUUGAGCAGAAA	| Symbols: ATEXPA4, ATEXP4, AT	11	0.205655535
AT4G35230.1_375	AT4G35230.1	375	2.534653465	0.947271045	1.740962255	1.226347305	3.531034483	2.378690894	ath-miR830-5p	3	1	22	388	409	UCUUCUCCAAAUAGUUUAGGUU	AGCCUAAACAAUUUGCGGAAGA	| Symbols: BSK1 | BR-signaling kinas	13	1.366308136
AT4G25210.1_567	AT4G25210.1	567	1.199674002	2.07	1.634837001	0.678341014	1.483870968	1.081105991	ath-miR864-3p	2	1	22	578	599	UAAAGUCAAUAAUACCUUGAAG	CUUCAAGGUAUUAUUGAUUUCA	| Symbols: | DNA-binding storekeeper	11	0.661292832
AT2G36380.1_859	AT2G36380.1	859	0.501207313	2.745209177	1.623208245	1.342883549	0.602404643	0.972644096	ath-miR773b-3p	2.5	1	21	871	891	UUUGAUUCCAGCUUUUGUCUC	GAGAGAGAAGCUGGAAUUAAG	| Symbols: PDR6, ATPDR6 | pleiotro	12	0.599210914
AT5G43780.1_383	AT5G43780.1	383	1.15354884	1.945519912	1.549534376	1.486922061	2.04505814	1.7659901	ath-miR395a	1.5	1	21	395	415	CUGAAGUGUUUGGGGGAACUC	GAGUUCCUCCAAACACUUCAU	| Symbols: APS4 | Pseudouridine synt	12	1.139690818
AT1G02130.1_140	AT1G02130.1	140	1.957569913	0.776587605	1.367078759	1.096309631	0.531413613	0.813861622	ath-miR5020a	3	1	21	152	172	UGGAAGAAGGUGAGACUUGCA	GGCAAGUCUUGUCUUCUUUUG	| Symbols: ATRAB1B, ARA5, ARA-	12	0.595328994
AT2G44620.1_102	AT2G44620.1	102	0.976976977	1.39399069	1.185483833	0.783209877	0.56612529	0.674667583	ath-miR869.1	3	1	21	116	136	AUUGGUUCAAUUCUGGUGUUG	AAACCCUAGGAUUGAAUCAGU	| Symbols: MTACP-1, MTACP1 | mi	14	0.569107367
AT1G77330.1_625	AT1G77330.1	625	1.237449615	1.105039267	1.171244441	1.815672745	1.601274993	1.708473869	ath-miR3933	2.5	1	21	639	659	AGAAGCAAAAUGACGACUCGG	AGGAGGUGUCGUUUUGCUUUU	| Symbols: | 2-oxoglutarate (2OG) and	14	1.458682585
AT1G35420.2_359	AT1G35420.2	359	1.891891892	0.343886463	1.117889177	2.154582763	0.837765957	1.49617436	ath-miR4228	2.5	1	21	371	391	AUAGCCUUGAACGCCGUCGUU	GUUGACGGUGUUGAAGGUUAU	| Symbols: | alpha/beta-Hydrolases sup	12	1.338392383
AT4G24090.1_838	AT4G24090.1	838	0.447024673	1.788617886	1.11782128	2.298507463	3.5	2.899253731	ath-miR2112-5p	2.5	1	21	850	870	CGCAAAUGCGGAUAUCAAUGU	GUCUUGAUAUUUGCGUUUGCG	| Symbols: | unknown protein; FUNC	12	2.593664823
AT3G55620.1_634	AT3G55620.1	634	0.957966764	1.237854644	1.097910704	0.258166491	1.272255193	0.765210842	ath-miR776	2.5	1	21	648	668	UCUAAGUCUUCUAUUGAUGUU	CACCUCAGUGGAAGACUUGGA	| Symbols: emb1624 | Translation initi	14	0.696970017
AT3G13470.1_315	AT3G13470.1	315	0.778745645	1.38841435	1.083579997	1.12090274	1.271873666	1.196388203	ath-miR833b	3	1	21	326	346	UGUUUGUUGACAUCGGUCUAG	UCAGACUGGUGUUAACAAGCU	| Symbols: | TCP-1/cpn60 chaperonin	11	1.104106948
AT1G35420.1_293	AT1G35420.1	293	1.815519766	0.332261522	1.073890644	2.06391478	0.809399478	1.436657129	ath-miR4228	2.5	1	21	305	325	AUAGCCUUGAACGCCGUCGUU	GUUGACGGUGUUGAAGGUUAU	| Symbols: | alpha/beta-Hydrolases sup	12	1.337805797
AT2G23610.1_823	AT2G23610.1	823	1.439781022	0.684895833	1.062338428	2.57122905	1.765100671	2.168164861	ath-miR5595a	2	1	21	836	856	ACAUAUGAUCUGCAUCUUUGC	UCAAAGACGCAGAUCAUAUGC	| Symbols: ATMES3, MES3 | methyl	13	2.040936113
AT5G25752.1_155	AT5G25752.1	155	1.34939759	0.602150538	0.975774064	5.78313253	2.028985507	3.906059019	ath-miR5653	3	1	24	169	191	UGGGUUGAGUUGAGUUGAGUUGG	GCCAACU-AACUCAACUCAACCCC	| Symbols: ATRBL11, RBL11 | rhom	14	4.00303632
AT1G20950.1_569	AT1G20950.1	569	1.063433644	0.830711991	0.947072817	1.632583998	0.590952839	1.111768419	ath-miR397a	3	1	21	583	603	UCAUUGAGUGCAGCGUUGAUG	GGUUAACGCUGCACUCAAAGC	| Symbols: | Phosphofructokinase fam	14	1.173899618
AT1G20225.1_319	AT1G20225.1	319	0.546948357	1.245989305	0.896468831	0	1.123794212	0.561897106	ath-miR169g-3p	3	1	21	333	353	UCCGGCAAGUUGACCUUGGCU	UGCCACGUUCAAUUUGCUGGA	| Symbols: | Thioredoxin superfamily	14	0.626789339
AT4G30170.1_871	AT4G30170.1	871	0.624127095	1.124567474	0.874347285	0.983172622	0.860167622	0.921670122	ath-miR5657	3	1	21	884	904	UGGACAAGGUUAGAUUUGGUG	CGUCAGAUCAAAUCUUGUUCA	| Symbols: | Peroxidase family protein	13	1.054123617
AT4G34920.1_914	AT4G34920.1	914	0.728244275	0.98027127	0.854257772	0.903409091	0.297752809	0.60058095	ath-miR5665	3	1	21	928	948	UUGGUGGACAAGAUCUGGGAU	GUUGCAGAUUUUGUCCACUGA	| Symbols: | PLC-like phosphodiestera	14	0.703044174
AT3G17185.1_206	AT3G17185.1	206	0.78125	0.919117647	0.850183824	0	0	0	ath-miR390a	3	1	21	217	237	AAGCUCAGGAGGGAUAGCGCC	GGUGUUAUCCUAUCUGAGCUU	| Symbols: TASIR-ARF, TAS3, ATT	11	0
AT5G26830.1_1294	AT5G26830.1	1294	0.83756645	0.852778446	0.845172448	0.417304297	0	0.208652148	ath-miR173-3p	3	1	21	1306	1326	UGAUUCUCUGUGUAAGCGAAA	GUUCGCUCAUAUAGAGAGUUA	| Symbols: | Threonyl-tRNA synthetas	12	0.246875237
AT4G22220.1_419	AT4G22220.1	419	0.504341261	1.121163683	0.812752472	2.36438152	1.343678161	1.854029841	ath-miR5654-3p	2.5	1	23	432	454	UGGAAGAUGCUUUGGGAUUUAUU	CCGAAAUCGCAAAGCAUCUUUCU	| Symbols: ISU1, ATISU1 | SufE/Nif	13	2.281174041
AT3G28200.1_658	AT3G28200.1	658	0.937288136	0.646878199	0.792083167	1.187969925	0.204795852	0.696382889	ath-miR5629	3	1	22	671	692	UUAGGGUAGUUAACGGAAGUUA	AAGCUUGUGCUAAUUACCCUAA	| Symbols: | Peroxidase superfamily p	13	0.879179002
AT3G62680.1_660	AT3G62680.1	660	0.742632368	0.801694414	0.772163391	0.680237612	0.625874825	0.653056219	ath-miR5595a	2.5	1	21	672	692	ACAUAUGAUCUGCAUCUUUGC	GCAAAGAUACAGAUUGUGUGU	| Symbols: PRP3, ATPRP3 | proline-r	12	0.845748745
AT1G76140.2_811	AT1G76140.2	811	0.349668874	1.128205128	0.738937001	2.312891114	1.508571429	1.910731271	ath-miR823	3	1	21	823	843	UGGGUGGUGAUCAUAUAAGAU	UUUUUCUAUGGUCGCUACCCA	| Symbols: | Prolyl oligopeptidase fam	12	2.585783725
AT1G76140.1_811	AT1G76140.1	811	0.342229875	1.098066298	0.720148087	2.266802444	1.486907731	1.876855087	ath-miR823	3	1	21	823	843	UGGGUGGUGAUCAUAUAAGAU	UUUUUCUAUGGUCGCUACCCA	| Symbols: | Prolyl oligopeptidase fam	12	2.606207142
AT2G36310.1_1038	AT2G36310.1	1038	0.79245283	0.631578947	0.712015889	1.817307692	0.939422181	1.378364937	ath-miR5652	3	1	21	1049	1069	UUGAAUGUGAAUGAAUCGGGC	GCCUGAUUUAUUCACAUAUAA	| Symbols: URH1 | uridine-ribohydrol	11	1.93586261
AT3G13470.1_312	AT3G13470.1	312	1.038779956	0.369612403	0.70419618	0.800214823	0.508098892	0.654156857	ath-miR833b	3	1	21	326	346	UGUUUGUUGACAUCGGUCUAG	UCAGACUGGUGUUAACAAGCU	| Symbols: | TCP-1/cpn60 chaperonin	14	0.928941218
AT4G09010.1_953	AT4G09010.1	953	0.757414999	0.63377724	0.695596119	1.02446184	0.306274682	0.665368261	ath-miR5630a	2	1	21	967	987	GCUAAGAGCGGUUCUGAUGGA	UGCAACAGAACAGCUCUUAGC	| Symbols: APX4, TL29 | ascorbate pe	14	0.956543952
AT4G27700.1_538	AT4G27700.1	538	0.533878107	0.833377624	0.683627866	1.628597395	1.537757437	1.583177416	ath-miR835-3p	3	1	21	551	571	UGGAGAAGAUACGCAAGAAAG	CUUUCUUUGGUAUCUUCUCUG	| Symbols: | Rhodanese/Cell cycle con	13	2.315846816
AT5G25752.1_158	AT5G25752.1	158	1.34939759	0	0.674698795	1.901528014	2.028985507	1.96525676	ath-miR5653	3	1	24	169	191	UGGGUUGAGUUGAGUUGAGUUGG	GCCAACU-AACUCAACUCAACCCC	| Symbols: ATRBL11, RBL11 | rhom	11	2.91279127
AT1G01320.1_649	AT1G01320.1	649	0.547643234	0.723837912	0.635740573	0.11765091	1.133897022	0.625773966	ath-miR394a	3	1	20	661	680	UUGGCAUUCUGUCCACCUCC	GGAGGUGGAAAGAAUUCUAA	| Symbols: | Tetratricopeptide repeat (T	12	0.984322839
AT1G01320.2_656	AT1G01320.2	656	0.545149481	0.721728595	0.633439038	0.117057513	1.130583323	0.623820418	ath-miR394a	3	1	20	668	687	UUGGCAUUCUGUCCACCUCC	GGAGGUGGAAAGAAUUCUAA	| Symbols: | Tetratricopeptide repeat (T	12	0.98481524
AT1G16720.1_1829	AT1G16720.1	1829	0.964516129	0.279113186	0.621814657	1.287405813	1.188866799	1.238136306	ath-miR868-3p	3	1	21	1841	1861	CUUCUUAAGUGCUGAUAAUGC	GCUUUAUCUGUACUUGAGAAG	| Symbols: HCF173 | high chlorophyl	12	1.991166164
AT1G20950.1_572	AT1G20950.1	572	0.93030303	0.311253802	0.620778416	1.037913547	1.57840617	1.308159859	ath-miR397a	3	1	21	583	603	UCAUUGAGUGCAGCGUUGAUG	GGUUAACGCUGCACUCAAAGC	| Symbols: | Phosphofructokinase fam	11	2.107289533
AT2G46800.1_292	AT2G46800.1	292	0.511897106	0.724294813	0.61809596	0.394254581	1.199698568	0.796976575	ath-miR856	1	1	22	304	325	UAAUCCUACCAAUAACUUCAGC	GUUGAAGUUGUUGGUGGGAUUA	| Symbols: ZAT, ATMTP1, MTP1, Z	12	1.289405896
AT2G46800.2_412	AT2G46800.2	412	0.509277031	0.718735892	0.614006461	0.392698569	1.189835575	0.791267072	ath-miR856	1	1	22	424	445	UAAUCCUACCAAUAACUUCAGC	GUUGAAGUUGUUGGUGGGAUUA	| Symbols: ZAT, ATMTP1, MTP1, Z	12	1.288695025
AT4G02510.1_3727	AT4G02510.1	3727	0.461609337	0.749812921	0.605711129	3.706535142	1.501998668	2.604266905	ath-miR5644	3	1	20	3739	3758	GUGGGUUGCGGAUAACGGUA	UACCGAUAUCUGGAACCCAC	| Symbols: TOC159, TOC86, PPI2, T	12	4.299519657
AT3G55620.1_637	AT3G55620.1	637	0.238791423	0.951086957	0.59493919	0.258166491	1.272255193	0.765210842	ath-miR776	2.5	1	21	648	668	UCUAAGUCUUCUAUUGAUGUU	CACCUCAGUGGAAGACUUGGA	| Symbols: emb1624 | Translation initi	11	1.286200094
AT1G52070.1_342	AT1G52070.1	342	0.642365537	0.546875	0.594620268	0	0.184372256	0.092186128	ath-miR846	2.5	1	21	354	374	UUGAAUUGAAGUGCUUGAAUU	GAUGCAAGCACUUGAAUUCAA	| Symbols: | Mannose-binding lectin s	12	0.155033612
AT3G49010.5_60	AT3G49010.5	60	0.408484129	0.705736251	0.55711019	0.6109375	1.220373747	0.915655623	ath-miR5662	2.5	1	20	74	93	AGAGGUGACCAUUGGAGAUG	UAUCCCCAAUGGUCACUUCA	| Symbols: ATBBC1, BBC1, RSU2 |	14	1.643580821
AT1G20225.1_322	AT1G20225.1	322	0.273153576	0.829181495	0.551167535	1.243329776	0.373397436	0.808363606	ath-miR169g-3p	3	1	21	333	353	UCCGGCAAGUUGACCUUGGCU	UGCCACGUUCAAUUUGCUGGA	| Symbols: | Thioredoxin superfamily	11	1.466638643
AT3G09050.1_633	AT3G09050.1	633	1.09787234	0	0.54893617	2.291296625	1.675324675	1.98331065	ath-miR865-3p	3	1	21	645	665	UUUUUCCUCAAAUUUAUCCAA	UUGGCUGAGUUUGAGGAGAAG	| Symbols: | unknown protein; FUNC	12	3.613007774
AT3G49010.4_62	AT3G49010.4	62	0.385390428	0.688235294	0.536812861	0.592648731	1.193181818	0.892915274	ath-miR5662	2.5	1	20	76	95	AGAGGUGACCAUUGGAGAUG	UAUCCCCAAUGGUCACUUCA	| Symbols: ATBBC1, BBC1, RSU2 |	14	1.663364161
AT1G48410.2_500	AT1G48410.2	500	0.686723349	0.384122919	0.535423134	1.597826087	0.3125	0.955163043	ath-miR168a	3	1	21	511	531	UCGCUUGGUGCAGGUCGGGAA	UUCCCGAGCUGCAUCAAGCUA	| Symbols: AGO1 | Stabilizer of iron t	11	1.783940556
AT1G48410.3_510	AT1G48410.3	510	0.686723349	0.384122919	0.535423134	1.597826087	0.3125	0.955163043	ath-miR168a	3	1	21	521	541	UCGCUUGGUGCAGGUCGGGAA	UUCCCGAGCUGCAUCAAGCUA	| Symbols: AGO1 | Stabilizer of iron t	11	1.783940556
AT1G48410.1_500	AT1G48410.1	500	0.686612798	0.383251051	0.534931924	1.6	0.312183497	0.956091749	ath-miR168a	3	1	21	511	531	UCGCUUGGUGCAGGUCGGGAA	UUCCCGAGCUGCAUCAAGCUA	| Symbols: AGO1 | Stabilizer of iron t	11	1.787314806
AT5G18800.1_117	AT5G18800.1	117	0.121979287	0.919961427	0.520970357	0.671594509	0.30070922	0.486151864	ath-miR5656	3	1	21	131	151	ACUGAAGUAGAGAUUGGGUUU	AAACCCGAUCCCUACUUCGGC	| Symbols: | Cox19-like CHCH family	14	0.933166078
AT5G18800.2_116	AT5G18800.2	116	0.121979287	0.919961427	0.520970357	0.671594509	0.30070922	0.486151864	ath-miR5656	3	1	21	130	150	ACUGAAGUAGAGAUUGGGUUU	AAACCCGAUCCCUACUUCGGC	| Symbols: | Cox19-like CHCH family	14	0.933166078
AT3G49010.1_72	AT3G49010.1	72	0.362960063	0.653755391	0.508357727	0.568650984	1.146993318	0.857822151	ath-miR5662	2.5	1	20	86	105	AGAGGUGACCAUUGGAGAUG	UAUCCCCAAUGGUCACUUCA	| Symbols: ATBBC1, BBC1, RSU2 |	14	1.687438011
AT3G49010.2_62	AT3G49010.2	62	0.362960063	0.653755391	0.508357727	0.568650984	1.146993318	0.857822151	ath-miR5662	2.5	1	20	76	95	AGAGGUGACCAUUGGAGAUG	UAUCCCCAAUGGUCACUUCA	| Symbols: ATBBC1, BBC1, RSU2 |	14	1.687438011
AT3G49010.3_87	AT3G49010.3	87	0.362960063	0.653755391	0.508357727	0.568650984	1.146993318	0.857822151	ath-miR5662	2.5	1	20	101	120	AGAGGUGACCAUUGGAGAUG	UAUCCCCAAUGGUCACUUCA	| Symbols: ATBBC1, BBC1, RSU2 |	14	1.687438011
AT4G09010.1_956	AT4G09010.1	956	0.504578313	0.492739008	0.49865866	1.195790504	0.92043956	1.058115032	ath-miR5630a	2	1	21	967	987	GCUAAGAGCGGUUCUGAUGGA	UGCAACAGAACAGCUCUUAGC	| Symbols: APX4, TL29 | ascorbate pe	11	2.121922502
AT1G69740.2_637	AT1G69740.2	637	0.506180106	0.467035951	0.486608028	0.281782438	1.18387414	0.732828289	ath-miR4221	2.5	1	22	650	671	UUUUCCUCUGUUGAAUUCUUGC	UGAAGAAUUCAACAGGGGAUGA	| Symbols: HEMB1 | Aldolase superfa	13	1.505993008
AT1G69740.1_681	AT1G69740.1	681	0.502806361	0.464212458	0.48350941	0.27928123	1.178543461	0.728912345	ath-miR4221	2.5	1	22	694	715	UUUUCCUCUGUUGAAUUCUUGC	UGAAGAAUUCAACAGGGGAUGA	| Symbols: HEMB1 | Aldolase superfa	13	1.507545315
AT1G66670.1_795	AT1G66670.1	795	0.275769746	0.638869745	0.457319745	0.232330827	0	0.116165414	ath-miR397a	3	1	21	809	829	UCAUUGAGUGCAGCGUUGAUG	GAUCGACGCUGUAAUCGAUGA	| Symbols: CLPP3, NCLPP3 | CLP pr	14	0.254013553
AT4G22220.1_418	AT4G22220.1	418	0.314856712	0.47866242	0.396759566	0.615781711	0.09526526	0.355523485	ath-miR5654-3p	2.5	1	23	432	454	UGGAAGAUGCUUUGGGAUUUAUU	CCGAAAUCGCAAAGCAUCUUUCU	| Symbols: ISU1, ATISU1 | SufE/Nif	14	0.896067834
AT4G17340.1_795	AT4G17340.1	795	0.270379884	0.5225624	0.396471142	0.218277066	0.425894378	0.322085722	ath-miR3440b-3p	2.5	1	21	806	826	UGGAUUGGUCAAGGGAAGCGU	AAGCUACCCUUGAUCAAUCCU	| Symbols: TIP2;2, DELTA-TIP2 | tor	11	0.812381251
AT1G52070.1_343	AT1G52070.1	343	0.401171676	0.312267658	0.356719667	0.433526012	0.646248535	0.539887273	ath-miR846	2.5	1	21	354	374	UUGAAUUGAAGUGCUUGAAUU	GAUGCAAGCACUUGAAUUCAA	| Symbols: | Mannose-binding lectin s	11	1.513477733
AT5G13630.2_3554	AT5G13630.2	3554	0.392292254	0.277216857	0.334754555	0.827455177	0.205307433	0.516381305	ath-miR395a	2	1	21	3567	3587	CUGAAGUGUUUGGGGGAACUC	GAGUUUUCUCAAACGCUUCAG	| Symbols: GUN5, CCH, CHLH, CCI	13	1.542566924
AT5G13630.1_3554	AT5G13630.1	3554	0.387302067	0.270180381	0.328741224	0.72603964	0.18559957	0.455819605	ath-miR395a	2	1	21	3567	3587	CUGAAGUGUUUGGGGGAACUC	GAGUUUUCUCAAACGCUUCAG	| Symbols: GUN5, CCH, CHLH, CCI	13	1.386560529
AT1G77330.1_626	AT1G77330.1	626	0.448830409	0.200326264	0.324578337	0.37650233	0.177098356	0.276800343	ath-miR3933	2.5	1	21	639	659	AGAAGCAAAAUGACGACUCGG	AGGAGGUGUCGUUUUGCUUUU	| Symbols: | 2-oxoglutarate (2OG) and	13	0.852799807
AT5G13630.2_3553	AT5G13630.2	3553	0.362107275	0.277216857	0.319662066	0.579104803	0.307986182	0.443545493	ath-miR395a	2	1	21	3567	3587	CUGAAGUGUUUGGGGGAACUC	GAGUUUUCUCAAACGCUUCAG	| Symbols: GUN5, CCH, CHLH, CCI	14	1.387544972
AT5G54810.1_450	AT5G54810.1	450	0.461916462	0.170846965	0.316381713	0.742789411	1.582491582	1.162640497	ath-miR5642a	3	1	20	461	480	UCUCGCGCUUGUACGGCUUU	GGAGCAUUACAGGCGCGAGA	| Symbols: TSB1, TRPB, TRP2, ATT	11	3.674803087
AT5G13630.1_3553	AT5G13630.1	3553	0.357501888	0.270180381	0.313841134	0.508147603	0.278418064	0.393282833	ath-miR395a	2	1	21	3567	3587	CUGAAGUGUUUGGGGGAACUC	GAGUUUUCUCAAACGCUUCAG	| Symbols: GUN5, CCH, CHLH, CCI	14	1.253127109
AT1G69740.2_639	AT1G69740.2	639	0.252941176	0.373547616	0.313244396	0.281782438	0.337585868	0.309684153	ath-miR4221	2.5	1	22	650	671	UUUUCCUCUGUUGAAUUCUUGC	UGAAGAAUUCAACAGGGGAUGA	| Symbols: HEMB1 | Aldolase superfa	11	0.988634295
AT1G77330.1_627	AT1G77330.1	627	0.224251278	0.400914136	0.312582707	0.301128004	0.354401154	0.327764579	ath-miR3933	2.5	1	21	639	659	AGAAGCAAAAUGACGACUCGG	AGGAGGUGUCGUUUUGCUUUU	| Symbols: | 2-oxoglutarate (2OG) and	12	1.048569135
AT1G69740.1_683	AT1G69740.1	683	0.251256281	0.3712898	0.311273041	0.27928123	0.336068777	0.307675003	ath-miR4221	2.5	1	22	694	715	UUUUCCUCUGUUGAAUUCUUGC	UGAAGAAUUCAACAGGGGAUGA	| Symbols: HEMB1 | Aldolase superfa	11	0.988440896
AT1G23390.1_517	AT1G23390.1	517	0.247021944	0.364207802	0.305614873	0.094484412	0.867077465	0.480780939	ath-miR775	3	1	20	531	550	UUCGAUGUCUAGCAGUGCCA	UGGAGCUGUUCGACAUCGAA	| Symbols: | Kelch repeat-containing F	14	1.573159494
AT2G44620.1_104	AT2G44620.1	104	0.24278607	0.30704698	0.274916525	0	0.188126446	0.094063223	ath-miR869.1	3	1	21	116	136	AUUGGUUCAAUUCUGGUGUUG	AAACCCUAGGAUUGAAUCAGU	| Symbols: MTACP-1, MTACP1 | mi	12	0.342151942
AT2G20260.1_119	AT2G20260.1	119	0.226487997	0.276874116	0.251681057	0.124882556	0.382161187	0.253521871	ath-miR5631	2.5	1	21	131	151	UGGCAGGAAAGACAUAAUUUU	ACCAUUGUGUCUUUCUUGCCG	| Symbols: PSAE-2 | photosystem I su	12	1.007314078
AT5G43780.1_382	AT5G43780.1	382	0.493684211	0	0.246842105	0.742284358	0.679710145	0.710997251	ath-miR395a	1.5	1	21	395	415	CUGAAGUGUUUGGGGGAACUC	GAGUUCCUCCAAACACUUCAU	| Symbols: APS4 | Pseudouridine synt	13	2.88037266
AT4G27700.1_540	AT4G27700.1	540	0.07611281	0.415915119	0.246013965	0	0.38247012	0.19123506	ath-miR835-3p	3	1	21	551	571	UGGAGAAGAUACGCAAGAAAG	CUUUCUUUGGUAUCUUCUCUG	| Symbols: | Rhodanese/Cell cycle con	11	0.777334165
AT4G17340.1_792	AT4G17340.1	792	0.202730099	0.245639892	0.224184995	0.291120815	0.170183799	0.230652307	ath-miR3440b-3p	2.5	1	21	806	826	UGGAUUGGUCAAGGGAAGCGU	AAGCUACCCUUGAUCAAUCCU	| Symbols: TIP2;2, DELTA-TIP2 | tor	14	1.028848102
AT5G13180.1_807	AT5G13180.1	807	0.329842932	0.116236162	0.223039547	0.348869405	0.489954634	0.419412019	ath-miR1886.3	1	1	21	821	841	AAUUAAAGAUUUCAUCUUACU	UUUCAGAUGAAAUCUUUAAUU	| Symbols: ANAC083, VNI2, NAC0	11	1.880437907
AT1G74260.1_3345	AT1G74260.1	3345	0	0.436008677	0.218004338	3.378962536	1.834419817	2.606691177	ath-miR828	2.5	1	22	3357	3378	UCUUGCUUAAAUGAGUAUUCCA	GGGAUUACUCAUUUGAGUGAGA	| Symbols: PUR4 | purine biosynthesis	12	11.95706102
AT1G64150.1_570	AT1G64150.1	570	0.4342723	0	0.21713615	2.182890855	0	1.091445428	ath-miR835-3p	3	1	21	583	603	UGGAGAAGAUACGCAAGAAAG	CUUUCUUGCUUAUCUUUUUCU	| Symbols: | Uncharacterized protein fa	13	5.026548673
AT5G43060.1_495	AT5G43060.1	495	0.346297681	0.034603886	0.190450784	0.21304988	0.16722851	0.190139195	ath-miR396a	2	1	21	508	528	UUCCACAGCUUUCUUGAACUG	AAGAUCAAGGAAGCUGUGGGA	| Symbols: | Granulin repeat cysteine p	13	0.99836394
AT5G43060.1_495	AT5G43060.1	495	0.346297681	0.034603886	0.190450784	0.21304988	0.16722851	0.190139195	ath-miR396b	2	1	21	508	528	UUCCACAGCUUUCUUGAACUU	AAGAUCAAGGAAGCUGUGGGA	| Symbols: | Granulin repeat cysteine p	13	0.99836394
AT3G49010.5_63	AT3G49010.5	63	0.135919455	0.234524231	0.185221843	0.185422438	0.207833371	0.196627904	ath-miR5662	2.5	1	20	74	93	AGAGGUGACCAUUGGAGAUG	UAUCCCCAAUGGUCACUUCA	| Symbols: ATBBC1, BBC1, RSU2 |	11	1.061580542
AT3G49010.4_65	AT3G49010.4	65	0.128301887	0.228896945	0.178599416	0.180007563	0.203558956	0.191783259	ath-miR5662	2.5	1	20	76	95	AGAGGUGACCAUUGGAGAUG	UAUCCCCAAUGGUCACUUCA	| Symbols: ATBBC1, BBC1, RSU2 |	11	1.073817956
AT3G49010.1_75	AT3G49010.1	75	0.12084474	0.217458384	0.169151562	0.172735985	0.195724466	0.184230225	ath-miR5662	2.5	1	20	86	105	AGAGGUGACCAUUGGAGAUG	UAUCCCCAAUGGUCACUUCA	| Symbols: ATBBC1, BBC1, RSU2 |	11	1.089142914
AT3G49010.2_65	AT3G49010.2	65	0.12084474	0.217458384	0.169151562	0.172735985	0.195724466	0.184230225	ath-miR5662	2.5	1	20	76	95	AGAGGUGACCAUUGGAGAUG	UAUCCCCAAUGGUCACUUCA	| Symbols: ATBBC1, BBC1, RSU2 |	11	1.089142914
AT3G49010.3_90	AT3G49010.3	90	0.12084474	0.217458384	0.169151562	0.172735985	0.195724466	0.184230225	ath-miR5662	2.5	1	20	101	120	AGAGGUGACCAUUGGAGAUG	UAUCCCCAAUGGUCACUUCA	| Symbols: ATBBC1, BBC1, RSU2 |	11	1.089142914
AT4G30170.1_870	AT4G30170.1	870	0.226678291	0.101912825	0.164295558	0.736822218	0.286217525	0.511519872	ath-miR5657	3	1	21	884	904	UGGACAAGGUUAGAUUUGGUG	CGUCAGAUCAAAUCUUGUUCA	| Symbols: | Peroxidase family protein	14	3.113412664
AT4G17340.1_794	AT4G17340.1	794	0.135116876	0.184184676	0.159650776	0.072716696	0	0.036358348	ath-miR3440b-3p	2.5	1	21	806	826	UGGAUUGGUCAAGGGAAGCGU	AAGCUACCCUUGAUCAAUCCU	| Symbols: TIP2;2, DELTA-TIP2 | tor	12	0.227736744
AT2G21530.1_78	AT2G21530.1	78	0.168480451	0.127594628	0.14803754	0.413998019	0	0.20699901	ath-miR5658	0	1	21	89	109	AUGAUGAUGAUGAUGAUGAAA	UUUCAUCAUCAUCAUCAUCAU	| Symbols: | SMAD/FHA domain-con	11	1.398287288
AT3G62680.1_659	AT3G62680.1	659	0.117023928	0.153853716	0.135438822	0.090527838	0.06247505	0.076501444	ath-miR5595a	2.5	1	21	672	692	ACAUAUGAUCUGCAUCUUUGC	GCAAAGAUACAGAUUGUGUGU	| Symbols: PRP3, ATPRP3 | proline-r	13	0.564841327
AT1G69740.2_638	AT1G69740.2	638	0.05056444	0.140004341	0.095284391	0.234793054	0.084346803	0.159569929	ath-miR4221	2.5	1	22	650	671	UUUUCCUCUGUUGAAUUCUUGC	UGAAGAAUUCAACAGGGGAUGA	| Symbols: HEMB1 | Aldolase superfa	12	1.674670188
AT1G69740.1_682	AT1G69740.1	682	0.050227777	0.139158576	0.094693177	0.232709168	0.083967975	0.158338571	ath-miR4221	2.5	1	22	694	715	UUUUCCUCUGUUGAAUUCUUGC	UGAAGAAUUCAACAGGGGAUGA	| Symbols: HEMB1 | Aldolase superfa	12	1.67212229
AT3G49010.5_62	AT3G49010.5	62	0.045279669	0.108152686	0.076716177	0.052932019	0.034599729	0.043765874	ath-miR5662	2.5	1	20	74	93	AGAGGUGACCAUUGGAGAUG	UAUCCCCAAUGGUCACUUCA	| Symbols: ATBBC1, BBC1, RSU2 |	12	0.570490804
AT3G49010.4_64	AT3G49010.4	64	0.042749371	0.105580954	0.074165163	0.051398337	0.033898305	0.042648321	ath-miR5662	2.5	1	20	76	95	AGAGGUGACCAUUGGAGAUG	UAUCCCCAAUGGUCACUUCA	| Symbols: ATBBC1, BBC1, RSU2 |	12	0.575045204
AT3G11120.1_80	AT3G11120.1	80	0.076103501	0.065019506	0.070561503	0.287162162	0.162601626	0.224881894	ath-miR831	2.5	1	22	94	115	UGAUCUCUUCGUACUCUUCUUG	GAAGAAGCGUAUGAGGAGAUUA	| Symbols: | Ribosomal protein L41 fa	14	3.187033773
AT3G49010.1_74	AT3G49010.1	74	0.040265833	0.100308391	0.070287112	0.049323596	0.032594937	0.040959267	ath-miR5662	2.5	1	20	86	105	AGAGGUGACCAUUGGAGAUG	UAUCCCCAAUGGUCACUUCA	| Symbols: ATBBC1, BBC1, RSU2 |	12	0.582742203
AT3G49010.2_64	AT3G49010.2	64	0.040265833	0.100308391	0.070287112	0.049323596	0.032594937	0.040959267	ath-miR5662	2.5	1	20	76	95	AGAGGUGACCAUUGGAGAUG	UAUCCCCAAUGGUCACUUCA	| Symbols: ATBBC1, BBC1, RSU2 |	12	0.582742203
AT3G49010.3_89	AT3G49010.3	89	0.040265833	0.100308391	0.070287112	0.049323596	0.032594937	0.040959267	ath-miR5662	2.5	1	20	101	120	AGAGGUGACCAUUGGAGAUG	UAUCCCCAAUGGUCACUUCA	| Symbols: ATBBC1, BBC1, RSU2 |	12	0.582742203
AT2G20260.1_118	AT2G20260.1	118	0.08336071	0.030711663	0.057036186	0.090802348	0.080287929	0.085545139	ath-miR5631	2.5	1	21	131	151	UGGCAGGAAAGACAUAAUUUU	ACCAUUGUGUCUUUCUUGCCG	| Symbols: PSAE-2 | photosystem I su	13	1.499839733
AT2G20260.1_117	AT2G20260.1	117	0.047622958	0.040951776	0.044287367	0.090802348	0.02006365	0.055432999	ath-miR5631	2.5	1	21	131	151	UGGCAGGAAAGACAUAAUUUU	ACCAUUGUGUCUUUCUUGCCG	| Symbols: PSAE-2 | photosystem I su	14	1.251666185
AT3G22890.1_429	AT3G22890.1	429	0	0.085047759	0.04252388	0.437067338	0.611355634	0.524211486	ath-miR395a	3	1	21	442	462	CUGAAGUGUUUGGGGGAACUC	GAGUUCCUCCAAACUCUUCAU	| Symbols: APS1 | ATP sulfurylase 1	13	12.32746146

Supplementary Table 2. List of TAS3 homologs.

Species	TAS3 homolog	Accession	Clade	Cleavable (Yes/No)	nts between stop codon and the 5´ end of miR390 binding site	ORF length	aa length
Arabidopsis thaliana	TAS3a	AT3G17185	eudicots	No	6	153	50
Arabidopsis thaliana	TAS3b	AT5G49615	eudicots	No	10	129	42
Arabidopsis thaliana	TAS3c	AT5G57735	eudicots	No	9	150	49
Antirrhinum majus	TAS3	AJ797948.1	eudicots	No?	3	195	64
Burma mangrove	TAS3	BP947370.1	eudicots	No?	9	213	70
Glycine max	TAS3	BE330988.1	eudicots	No?	3	168	55
Gossypium raimondii	TAS3	CO077318.1	eudicots	Yes?	10	132	43
Manihot esculenta	TAS3	CK652751	eudicots	No?	3	102	33
Mesembryanthemum crystallinum	TAS3	BF479835.1	eudicots	No?	9	135	44
Populus trichocarpa	TAS3	DT498974.1	eudicots	No?	6	171	56
Solanum lycopersicum	TAS3-1	NR_138079.1	eudicots	No?	62	99	32
Solanum lycopersicum	TAS3-12	JX047547.1	eudicots	Yes?/No?	10	99	32
Swingle citrumelo	TAS3	CX663477.1	eudicots	No?	3	156	51
Theobroma cacao	TAS3	CA795323.1	eudicots	No?	3	114	37
Vitis vinifera	TAS3	DT025007.1	eudicots	No?	3	180	59
Pinus taeda	TAS3	DR112999.1	Gymnosperm	Yes	ORF	129	42
Hordeum vulgare	TAS3	BF264964.3	Monocots	Yes?	10	213	70
Oryza sativa Japonica	TAS3	AU100890.1	Monocots	No?	9	114	37
Saccharum	TAS3	CA145655.1	Monocots	Yes?	ORF	120	39
Sorghum bicolor	TAS3	CD464142.1	Monocots	No?	9	141	46
Triticum aestivum	TAS3	CN010916.1	Monocots	No?	9	177	58
Zea mays	TAS3	BE519095.1	Monocots	Yes?	14	126	41
Physcomitrella patens	TAS3a	BK005825	moss	Yes?	10	162	53
Physcomitrella patens	TAS3b	BK005826	moss	Yes?	nd		
Physcomitrella patens	TAS3c	BK005827	moss	Yes?	nd		
Physcomitrella patens	TAS3d	BK005828	moss	Yes?	nd		

? (predicted from sequence)

Supplementary Table 3. List of synthetic RNA oligos used in this study.

Name	Sequence (5′-3′)
miR390(21 nt)-guide	AAGCUCAGGAGGGAUAGCGCC(M)
miR390(21 nt)-passenger	CGCUAUCCAUCCUGAGUUUCA(M)
miR390(20 nt)-guide	AAGCUCAGGAGGGAUAGCGC(M)
miR390(20 nt)-passenger	GCUAUCCAUCCUGAGUUUCA(M)
miR390_21_4SU	AAGCUCAGGAGGGAUAGCGC4(M)
miR173(22 nt)-guide	UUCGCUUGCAGAGAGAAAUCAC(M)
miR173(22 nt)-passenger	GAUUCUCUGUGUAAGCGAACA(M)
miR173(21 nt)-guide	UUCGCUUGCAGAGAGAAAUCA(M)
miR173(21 nt)-passenger	AUUUCUCUCAGCAACGCAUAG(M)

"(M)" indicates 2′-OMe modification.

Supplementary Table 4. List of synthetic DNA oligos and long fragments used in this study.

Name	Sequence (5′-3′)
T7_ADH_5UTR_*3×HA*	ATGCCTGCAGGTCGACTCTAGATAATACGACTCACTATAGGGT ACATCACAATCACACAAAACTAACAAAAGATCAAAAGCAAGT TCTTCACTGTTGATAatgGTTTACCCATACGATGTTCCTGACTATG CGGGCTATCCCTATGACGTCCCGGACTATGCAGGATCCTATCC ATATGACGTTCCAGATTACGCTCCGTGGCGCGCCAGCTTGAGA
T7_TAS3a	CCGCGGTAATACGACTCACTATAGGATCCCACCGTTTCTTAAG ACTCTCTCTCTTTCTGTTTTCTATTTCTCTCTCTCTCAAATGAAAG AGAGAGAAGAGCTCCCATGGATGAAATTAGCGAGACCGAAGT TTCTCCAAGGCATTAAGGAAAACATAACCTCCGTGATGCATAG AGATTATTGGATCCGCTGTGCTGAGACATTGAGTTTTTCTTCGG CATTCCAGTTTCAATGATAAAGCGGTGTTATCCTATCTGAGCTT TTAGTCGGATTTTTTCTTTTCAATTATTGTGTTTTATCTAGATGAT GCATTTCATTATTCTCTTTTTCTTGACCTTGTAAGGCCTTTTCTTG ACCTTGTAAGACCCCATCTCTTTCTAAACGTTTTATTATTTTCTC GTTTTACAGATTCTATTCTATCTCTTCTCAATATAGAATAGATAT CTATCTCTACCTCTAATTCGTTCGAGTCATTTTCTCCTACCTTGTC TATCCCTCCTGAGCTAATCTCCACATATATCTTTTGTTTGTTATT GATGTATGGTTGACATAAATTCAATAAAGAAGTTGACGTTTTT CTCTCGAG
TAS3aPDS2	TTCATTTGGAGAGGCTCGAGGTCGACATCCCACCGTTTCTTAAG ACTCTCTCTCTTTCTGTTTTCTATTTCTCTCTCTCTCAAATGAAAG AGAGAGAAGAGCTCCCATGGATGAAATTAGCGAGACCGAAGT TTCTCCAAGGTGATATGTCTATCTGTATATGTGATACGAAGAGT TAGGGTTTTGTCATTTCGAAGTCAATTTTTGTTTGTTTGTCAATA ATGATATCTGAATGATGAAGAACACGTAACTAAGATATGTTAC TGAACTATATAATACATATGTGTGTTTTTCTGTATCTATTTCTAT ATATATGTAGATGTAGTGTAAGTCTGTTATATAGACATTATTCA TGTGTACATGCATTATACCAACATAAATTTGTATCAATACTACT TTTGATTTACGATGATGGATGTTCTTAGATATCTTCATACGTTTG TTTCCACATGTATTTACAACTACATATATATATTTGGAATCACATA TATACTTGATTATTATAGTTGTAAAGAGTAACAAGTTCTTTTTTC AGGCATTAAGGAAAACATAACCTCCGTGATGCATAGAGATTA TTGGATCCGCTGTGCTGAGACATTGAGTTTTTCTTCGGCATTCC AGTTTCAATGATAAAGCGGTGTTATCCTATCTGAGCTTTTAGTC GGATTTTTTCTTTTCAATTATTGTGTTTTATCTAGATGATGCATTT CATTATTCTCTTTTAAGTAGCACTTCCCCACCTATTGAGAAGTG GGAACCCTAAAATCTCTTTCTAAACGTTTTATTATTTTCTCGTTT TACAGATTCTATTCTATCTCTTCTCAATATAGAATAGATATCTAT CTCTACCTCTAATTCGTTCGAGTCATTTTCTCCTACCTTGTCTATC CCTCCTGAGCTAATCTCCACATATATCTTTTGTTTGTTATTGATG TATGGTTGACATAAATTCAATAAAGAAGTTGACGTTTTTCTACT AGTTCTAGACGCTGAAATCACCA
oligoK1	GAACAGATTGGAGGTATGAGTTCTAGGGCTGGTCCAATGTCTA A
oligoK2	CCATGGGACGTCGACCTGAGGTAATTATAACCCTCAATCATCT TCATTGTGAAGGCCATGCT
oligoE1	GCTGGCGCGCCATGGAAGAAAAAACTCATCATCATCATCAC
oligoE2	GCTGGCGCGCCTCAGCAGTAAAACATGAGATTCTTGAC
oligo512	CTTGTCATCGTCATCCTTGTAATCGATGTCATGATCTTTATAATC ACCGTCATGGTCTTTGTAGTC
oligo955	TATAGGGAGACCCAAGCTGGCGCGCCATGGACTACAAAGACC
oligo1039	ACCTCCAATCTGTTCGCGGT
oligo1044	AACCACCTATCTACATCACCAAGATATGGGACATCATCATCAT CATCACATGGACGAGAAGACCACCGG
oligo1062	CTCGCGAATGCATCTAGATCCGCGGTAATACGACTCACTATAG GA
oligo1063	TTGAGAGAGAGAGAAATAGA
oligo1064	GTTTTCTATTTCTCTCTCTCTCAAATGGACTACAAAGACCATGA CGG
oligo1065	CGATTACAAGGATGACGATGACAAGATGAAAGAGAGAGAAG AGCTCC
oligo1066	GTCGACGGGCCCGGGATCCGATCTCGAGAGAAAAACGTCAAC TTCTTTATTGAAT
oligo1073	TGGAGATTTCGAGTCGAGGGATAGACAAGGTAGGA
oligo1074	GACTCGAAATCTCCACATATATCTTTTGTTTGTTA
oligo1094	CCAAAAGTCTCAAGCTGGCGCGCCTCAGCAGTAGAACATGAC AC
oligo1096	AAAAGTCTCAAGCTGGCGCGCCTCAGACGAAGAACATAACAT TC
oligo1099	TTCGAGTCATAGGATAACACCGCTTTATCATTGAAACTGGAAT G
oligo1100	ATCCTATGACTCGAATTAGTCGGATTTTTTCTTTTCAATT
oligo1101	AAGCTCAGATAGGATAACACGGCTTTATCATTGAAACTGGAAT G
oligo1102	ATCCTATCTGAGCTTTTAGTCGGATTTTTTCTTTTCAATT
oligo1104	AAGCTCAGATAGGATAGCGCCGCTTTATCATTGAAACTGGAAT G
oligo1106	ATCCCTCCTGAGCTTTTAGTCGGATTTTTTCTTTTCAATT
oligo1107	AAGCTCAGGAGGGATAGCGCCGCTTTATCATTGAAACTGGAAT G
oligo1118	TATAGGGAGACCCAAGCTGGCGCGCCCCTGCAGGATGTACCC ATACGATGTTCCAGATTACGCTTACCCATACGATGTTCCAGATT ACGCTTACCCATACGATGTTCCAGATTACGCTATGGTGAGAAA GAGAAGAACGG
oligo1119	TATAGGGAGACCCAAGCTGGCGCGCCCCTGCAGGATGTACCC ATACGATGTTCCAGATTACGCTTACCCATACGATGTTCCAGATT ACGCTTACCCATACGATGTTCCAGATTACGCTATGGAGAGAGG TGGTTATCG
oligo1159	ACACCCAAAAGTCTCAAGCTGGCGCGCCTCAGCAGTAAAACA TGAGAT
oligo1160	GGCTCACCGCGAACAGATTGGAGGTATGGAAGAAAAAACTCA TCATCATC
oligo1161	TTTCAATGATAATTAAGCGGTGTTATCCTATCTGA
oligo1162	TAATTATCATTGAAACTGGAATGCCGAAGAAAAAC
oligo1163	TTCAATGATAAGTTAAGCGGTGTTATCCTATCTGA
oligo1164	TAACTTATCATTGAAACTGGAATGCCGAAGAAAAA
oligo1165	TCAATGATAAAGTTAAGCGGTGTTATCCTATCTGA
oligo1166	TAACTTTATCATTGAAACTGGAATGCCGAAGAAAA
oligo1167	CAATGATAACAGTTAAGCGGTGTTATCCTATCTGA
oligo1168	TAACTGTTATCATTGAAACTGGAATGCCGAAGAAA
oligo1180	AGTTTCAATGATAAAAGCGGTGTTATCCTATCTGA
oligo1181	TTTATCATTGAAACTGGAATGCCGAAGAAAAACTC
oligo1182	GTTTCAATGATAATAAGCGGTGTTATCCTATCTGA
oligo1183	TATTATCATTGAAACTGGAATGCCGAAGAAAAACT
oligo1197	TTCTCTCTCTCTCAAATGAAAGAGAGAGAAGAGCTCC
oligo1198	TTGAGAGAGAGAGAAATAGAAAACAG
oligo1201	GACTCTAGAGGATCCCCGGGTACCCTCGAGGTCGACATCCCAC C
oligo1202	GAGAATAATGAAATGCATCATCTAG
oligo1203	CTAGATGATGCATTTCATTATTCTC
oligo1204	GGTGGGCGGCCGCTCTAGAACTAGTTAATTAAGAATTATCGAA CCACTT
oligo1205	GATAGGATAACACCGCTTAACTGTTTATCATTGAAACTGGAAT GCC
oligo1206	AACAGTTAAGCGGTGTTATCCTATCTGAGCTTTTA
oligo1207	CAGATAGGATAACACCGCTTAATTATCATTGAAACTGGAATGC C
oligo1208	TAATTAAGCGGTGTTATCCTATCTG
oligo1209	TTCGAGTCATAGGATAACACCGCTTTATCATTGAAACTGGAA
oligo1210	GCGGTGTTATCCTATGACTCGAATTAGTCGGATTTTTTCTTTTCA
oligo1211	TTATCACCATGGGAGCTCTTCTCTCT
oligo1212	AGAAGAGCTCCCATGGTGATAATTAGCGAGACCGAAGTTTCT
oligo1220	GCTTTATCATTGAAACTGGAATG
oligo1221	TTTCAATGATAAAGCAGTGTTATCCTATCTGAGCTT
oligoA1	AAACCTAAACCCCTAACGGC
oligoA2	TTACAATTTCAATATAAATGATATAATTTTTACA
oligoA3	AATTGGGCCCTCTAGATGCA
oligoA4	CACCGTCATGGTCTTTGTAGTCCATCTCACAAACTCGATCTCAA TCTAGC
oligoA5	ATGGACTACAAAGACCATGAC
oligoA6	TAGACAGGGATATCGAACCTAACATCTTGTCATCGTCATCCTTG T
oligoA7	ATGTTAGGTTCGATATCCCTGTCTATTTGTC
oligoA8	GCTTGGTACCGAGCTCGGAT
oligoA9	TAATACGACTCACTATAGGGAAACCTAAACCCCTAACGGCTAA GC
oligoA10	TTTTTTTTTTTTTTTTTTTTTTTTTTTTTTTTTTTTTTTTTTTTTTTT TTTTTTTTTGTAAAAATTATATCATTTATATTGAAATTGTAA
oligo1230	TCATTGAAACTGGAATGCCGAAGAAAAACTCAATGTCTCA
oligo1231	AAGAAAAACTCAATGTCTCAGCACAGCGGATCCAATAATC
oligo1232	GCACAGCGGATCCAATAATCTCTATGCATCACGGAGGTTA
oligo1233	TCTATGCATCACGGAGGTTATGTTTTCCTTAATGCCTTGG
oligo1234	TGTTTTCCTTAATGCCTTGGAGAAACTTCGGTCTCGCTAA
D7(+)_detection_probe	GGGGTCTTACAAGGTCAAGAA